MAPK/MAK/MRK overlapping kinase (MOK) controls microglial inflammatory/type-I IFN responses via Brd4 and is involved in ALS pathophysiology

Jesús A. Pérez-Cabello[#1,2], Jaime M. Franco[#1], Lucía Silvera-Carrasco[#1,2], Vivian Capilla-González[1], Alexandros Armaos[3], María Gómez-Lima[1], Raquel García-García[1,2], Xin Wen Yap[4], M. Magdalena Leal-Lasarte[1], Deepti Lall[5], Robert H. Baloh[5], Salvador Martínez[6], Yoshihiko Miyata[7], Gian G. Tartaglia[3,8], Ritwick Sawarkar[4], Mario García-Dominguez[1], David Pozo[1,2], Cintia Roodveldt[1,2]*

[#]these authors contributed equally to this work

[1]Andalusian Centre for Molecular Biology and Regenerative Medicine-CABIMER, Universidad de Sevilla-CSIC, Seville, Spain.

[2]Department of Medical Biochemistry, Molecular Biology and Immunology, University of Seville, Seville, Spain.

[3]Center for Human Technologies (CHT) and Center for Life Nano Science (CNLS), Istituto Italiano di Tecnologia (IIT), Genova, Italy.

[4]The Medical Research Council Toxicology Unit, University of Cambridge, Cambridge, UK.

[5]Department of Neurology, Cedars-Sinai Medical Center, Los Angeles, CA 90048, USA.

[6]Instituto de Neurociencias, Universidad Miguel Hernández de Elche-CSIC, Sant Joan d'Alacant, Spain.

[7]Department of Cell and Developmental Biology, Graduate School of Biostudies, Kyoto University, Kyoto 606-8502, Japan.

[8]Department of Biology and Biotechnologies, University Sapienza Rome, Rome, Italy

Abstract

Amyotrophic lateral sclerosis (ALS) is a fatal and incurable neurodegenerative disease affecting motor neurons and characterized by microglia-mediated neurotoxic inflammation whose underlying mechanisms remain incompletely understood. In this work we reveal that MAPK/MAK/MRK overlapping kinase (MOK), with unknown physiological substrate/s, displays an immune-related function, namely by controlling inflammatory and type-I IFN responses in microglia which result neurotoxic to primary motor neurons. Moreover, we uncover the epigenetic reader bromodomain-containing protein 4 (Brd4) as the first molecule regulated by MOK, by promoting Ser^{492}-phospho-Brd4 levels. We further demonstrate that MOK regulates Brd4 functions by supporting Brd4 binding to cytokine gene promoters, therefore enabling innate immune responses. Remarkably, we show that MOK levels are increased in ALS spinal cord, particularly in microglial cells, and that administration of a chemical MOK-inhibitor to ALS model mice can suppress microglial activation and delay disease onset, pointing to a pathophysiological role of MOK kinase in ALS and neuroinflammation.

Introduction

Amyotrophic lateral sclerosis (ALS) is a fatal adult-onset neurodegenerative disease in which motor neurons in the cortex, brain stem and spinal cord gradually degenerate and die off[1,2]. A typical characteristic of ALS and most other neurodegenerative diseases is neuroinflammation which is associated with disease progression and spreading[1]**.** In particular, several studies have shown that microglia, the main immunocompetent cells in the central nervous system (CNS), become activated and neurotoxic and thereby contribute to motor neuron loss and disease progression[3]. Still, the mechanisms driving microglia activation and neurotoxicity in ALS remain incompletely understood. Key molecular mediators along the activated signalling pathways that may serve as new therapeutic targets or disease biomarkers need to be identified[4–6]. A powerful emerging view poses that dysregulated neuroinflammatory responses in these disorders may be caused by disruption at the signalling-epigenetics-transcriptional axis level[7,8].

A hallmark of ALS and other related disorders is the intracellular accumulation of protein inclusions containing misfolded TDP-43 (transactive response DNA-binding protein-43) and in certain cases, RNA-binding protein FUS or SOD1 (superoxide dismutase 1) proteins. TDP-43 -a multifunctional protein with RNA/DNA binding activities and physiological localization in the cell nucleus- has been found to display functional abnormalities, including its identification as a major component of cytosolic intraneuronal and glial inclusions, in virtually all ALS patients[9,10] and a number of ALS animal models[11,12]. Thus, TDP-43 is currently thought to represent a common molecular hub in these disorders, where different pathogenic mechanisms may converge and finally result in neurotoxic cellular outcomes[13].

Recently, we found that MAPK/MAK/MRK overlapping kinase (MOK), a Ser/Thr kinase that belongs to the MAPK superfamily[14], interacts and co-localizes with cytosolic TDP-43 aggregates that are able to elicit a proinflammatory response in microglia[15]. MOK is an atypical Ser/Thr signalling kinase, found both in the cytosol and nucleus of different cell types and with a demonstrated function in cilium growth regulation in renal epithelium[16]. Up to now, no physiological substrate or downstream-regulated target have been identified for this kinase, and its functions and molecular mechanisms in relation to immunity or the central nervous system (CNS) have not been identified.

In this study, we uncover a role of MOK kinase in controlling inflammatory and type-I IFN responses in microglia via a Brd4 epigenetic-dependent mechanism and report that

MOK's immune-related functions are dysregulated, and actively participate, in ALS pathophysiology.

Results

MOK-mediated mechanisms are mobilized in microglial cells under TDP-43 aggregation

To evaluate whether MOK is engaged in cellular processes activated in the context of TDP-43 aggregation, we started by carrying out SLAM-Seq analysis to report on immediate changes in RNA synthesis[17] from microglial cells (SIM-A9) exposed to TDP-43 or sham aggregates, with or without pre-treatment with AG2P145D/Comp13 (C13) MOK inhibitor[18] **(Supplem. Figure 1a)**. C13 is an unusually specific inhibitor based on the structural, virtual uniqueness of a cysteine gatekeeper in MOK's active site[18]. The results showed a clear difference in the transcriptional changes caused by MOK-inhibition for a number of genes between the various conditions. Remarkably, pre-treatment with MOK-kinase inhibitor (C13) revealed a dramatically different impact in the number of the differentially expressed genes (DEGs) **(Figure 1a, Supplem. Figure 1b)** and their predicted interaction networks[19] under TDP-43 aggregation compared to control (sham)-treated cells **(Figure 1b)**. Interestingly, 45% of the differentially expressed genes resulting from exposure to TDP-43 aggregates were counter-regulated by C13 pre-treatment **(Figure 1c)**, suggesting a possible role of MOK in TDP-43 aggregates-elicited cellular responses.

Next, to identify proteins whose phosphorylation state could be regulated by MOK kinase in the ALS cellular model, we used IP against phospho-Ser/Thr-containing proteins from microglial cells exposed to TDP-43 aggregates, pre-treated or not with C13. By subsequent LC-MS/MS analyses of both eluates, we identified several proteins in both samples, a few of them exclusively in the absence of MOK inhibitor pre-treatment, including desmoplakin (Dsp), heat-shock protein 1-like protein (HSPA1L), bromodomain-containing protein 4 (Brd4) and apolipoprotein L 7a (Apol7a) **(Figure 1d)**. Taken together, these results indicate that MOK is functionally mobilized and may regulate downstream protein phosphorylation and signalling processes in microglial cells under TDP-43 aggregation.

MOK controls microglial responses by regulating inflammatory and type-I IFN pathways

To investigate a potential role of MOK in mediating the inflammatory response in microglia, we assessed TNFα, IL-6 and IL-1β cytokine secretion levels in culture supernatants

from lipopolysaccharide (LPS)-stimulated primary microglial cells (5 h or 16 h post-stimulation), either pre-treated or not with C13. Remarkably, C13-pre-treatment significantly reduced secretion of all three proinflammatory cytokines otherwise induced by LPS alone **(Figure 2a)**. This result was also observed for SIM-A9 microglial cells, in which pre-treatment of cells with C13 led to lower TNFα secreted levels after LPS stimulation **(Supplem. Figure 2a)**. Furthermore, Western blot analyses after LPS treatment resulted in lower Ser^{536} phosphorylation of p65 signal upon LPS stimulation for C13-pre-treated cells, pointing to a role of MOK in NF-κB pathway in the inflammatory response **(Supplem. Figure 2b)**. Next, to elucidate the effect of C13-treatment on LPS-stimulated primary microglia at a transcriptional level, RNA-Seq was carried out with RNA isolated from primary microglial cells after 5h-stimulation with LPS, subjected or not to pre-treatment with C13. Based on the 158 differentially expressed genes (DEGs) identified, we used Ingenuity Pathway Analysis (IPA) software enabling to predict canonical pathways, upstream regulators, functions and networks, among others **(Figure 2b)**. Notably, IPA revealed a number of significantly inhibited (IRF3/7, PML and STAT1) and activated (CEBPB, NFE2L2 and STAT3) upstream regulators as a result of C13 pre-treatment.

To confirm the participation of MOK in the inflammatory response in microglia, CRISPR/Cas9-generated MOK-KO and WT SIM-A9 cells **(**see **Supplem. Figure 2c,d)** were stimulated with LPS for 5 h and analyzed by qRT-PCR and/or ELISA for a set of key cytokines, namely IL-6, TNFα, IFN-β and IL-1α **(Figure 2c,d, Supplem. Figure 2e,f)**, the results clearly demonstrating reduced levels of all these cytokines in LPS-stimulated MOK-KO cells. As expected, this profile of cytokine expression was mirrored by flow cytometry analysis **(Figure 2e, left)**. Importantly, we assessed the functional restoration of MOK activity in MOK-KO cells transfected with a FLAG-MOK construct carrying or not a 'kinase-dead' (MOK-KD) mutation[20], of IL-6-expressing cells after LPS-stimulation **(Figure 2e, right)**. Remarkably, quantification of $IL\text{-}6^{+}$ cells in transfected cells (detected with anti-FLAG immunolabeling) demonstrated the rescuing of cytokine expression in MOK-KO cells by recombinant MOK-WT, but not by MOK-KD **(Figure 2e, Supplem. Figure 3a)**. Put together, these results demonstrate that MOK controls the inflammatory response in microglia and this function is dependent on its kinase activity. To assess the impact in neuronal viability of MOK-regulated microglial responses, we isolated primary motor neurons from mouse embryos for cell culture. We then exposed these cultured neurons to conditioned media from LPS-stimulated WT or MOK-KO cells, and quantified dead cells by using a fluorescence-

based assay **(Figure 2f)**. As expected, medium from LPS-stimulated WT cells caused a reduction in neuronal cell survival compared to control conditions. Notably, the opposite effect was seen with medium from LPS-stimulated MOK-KO cells, indicating that MOK-mediated microglial responses can be neurotoxic.

We then carried out RNA-Seq analysis by comparing MOK-KO vs. WT SIM-A9 cells, stimulated or not with 1 μg/mL LPS for 5 h **(Figure 3a,b and Supplem. Figure 4**. A relatively large number of protein-coding and non-coding DEGs were identified, showing partial overlap between both cell lines and treatments, and including 730 total DEGs **(Figure 3a, top)** and 424 coding DEGs **(Figure 3a, bottom, 3b)** found when comparing MOK-KO vs. WT cells stimulated with LPS. Gene ontology (GO) clustering analysis revealed significantly enriched biological processes related to microglial activation and innate immunity and, interestingly, IFNα/IFNβ (type-I IFN) regulation and antiviral responses **(Figure 3c,d, Supplem. Figure 5a)**. In particular, analysis of coding DEGs that differentially changed for MOK-KO or WT cells upon LPS-stimulation revealed enriched terms related to 'innate immunity', 'positive NF-κB regulation' and 'antiviral response' **(Figure 3c,d, Supplem. Figure 5b)**. Finally, ingenuity pathway analysis (IPA) prediction between MOK-KO vs. WT cells upon LPS stimulation unleashed a number of activated (CITED2, TRIM24) and inhibited (e.g. IRF7, STAT1, BHLHE40) upstream regulators **(Figure 3e)** as well as differentially regulated 'neuroinflammation', 'pyroptosis' and 'TRIM1' canonical pathways, among others **(Supplem. Figure 5c)**. The expression of interferon regulatory factor 7 (IRF7), a principal type-I IFN master regulator and also a DEG revealed in our RNA-Seq study, was assessed by qRT-PCR and confirmed to be suppressed in the MOK-KO cells upon LPS stimulation **(Figure 3f)**. Collectively, our results demonstrate a role of MOK in microglia activation and inflammatory response mediated by NF-κB and STAT1 pathways and critically involving induction of IRF7/type-I IFN and antiviral cellular responses.

MOK mediates the inflammatory response by regulating phospho-Brd4 levels and Brd4 chromatin-binding in microglia

One of the proteins whose phosphorylated state levels we found to be putatively regulated by MOK **(Figure 1c)** corresponds to the epigenetic reader Brd4 belonging to the BET bromodomain family, controlling the transcription of genes by binding to acetylated histones in chromatin[21]. Brd family members have been linked to cancer and autoimmune disease mechanisms that are still not clear. In particular, Brd4 has been recently involved in innate

immune responses, including inflammatory responses[22,23]. To verify that Brd4 is mediating the inflammatory response in microglial cells as previously shown[24,25], we stimulated SIM-A9 cells in culture with LPS for 5 h after pre-treatment with the Brd4 inhibitor (+)-JQ1 (or (-)-JQ1 negative control) and quantified IL-6 and TNFα secretion levels by ELISA, confirming that (+)-JQ1 effectively suppresses LPS-induced inflammatory responses in both primary microglia and SIM-A9 cells (**Supplem. Figure 6a,b).**

Next, to validate our screening result **(Figure 1d)** and test whether MOK kinase is regulating phosphorylated Brd4 levels in inflammatory microglia, we quantified Ser^{492} phosphorylated Brd4 (pBrd4) –previously shown to mediate Brd4 chromatin-binding functions[26,27]– in samples from C13-pretreated SIM-A9 cells stimulated with LPS by Western blot, showing a clear attenuation of the pBrd4 band (ca. 250 kDa) in LPS-stimulated cells, as a result of C13-pretreament **(Supplem. Figure 6c)**. Moreover, confocal immunofluorescence analyses with primary microglia showed that, contrary to LPS-stimulated cells displaying higher pBrd4 nuclear levels compared to basal control, C13-pretreatment led to lower pBrd4 nuclear levels following LPS stimulation **(Figure 4a,b).** Importantly, these results were mirrored by LPS-stimulated MOK-KO cells compared to WT cells both by Western blot **(Figures 4c,d and Supplem. Figure 2g)** and confocal immunofluorescence analysis **(Figure 4e,f)**, in which a significant reduction of nuclear pBrd4 was seen in MOK-KO compared to WT cells, upon LPS-stimulation. These results clearly demonstrate that MOK kinase regulates nuclear pBrd4 levels in microglia under inflammatory conditions.

To assess a possible role of MOK in Brd4 binding to key cytokine gene promoters previously linked to Brd4 recruitment[28–30], we carried out ChIP-qPCR assays from SIM-A9 cells after 1h-LPS stimulation **(Figure 4g)**. Remarkably, we found that whereas WT cells showed incremented Brd4 binding to IL-6 and IFNβ promoters in response to LPS compared to unstimulated cells, such increase was abrogated in MOK-KO cells for Il6, Ifnβ and, to a lesser extent, Tnfα. These results demonstrate a role of MOK in positive regulation of Brd4 binding to proinflammatory and type-I IFN gene promoters under inflammatory conditions. Of note, pre-treatment with the Brd4-inhibitor (+)-JQ1 resulted in significant reduction of the ChIP-qPCR signal increments, confirming the specificity of Brd4 binding assessment in our assays **(Supplem. Figure 6d)**. Collectively, these results reveal a central role for MOK in Brd4-mediated regulation of cytokine expression upon inflammatory stimulation.

MOK is altered in spinal cord from ALS patients and mouse model, and C13-administration to SOD1^{G93A} mice modifies disease course

Given that MOK was found to be engaged in microglia under TDP-43 aggregation and based on our results herein showing a role of MOK in the inflammatory response, we wondered whether MOK would be altered in ALS individuals. To address this question, we first assessed phospho-Ser^{159}/Tyr^{161} MOK (bpMOK) –considered to correspond to the fully active form of the kinase[14]- by Western blot using murine spinal cord tissue homogenates, observing a band of ca. 65 kDa, in agreement with previously reported MW for CNS tissue[31] **(Supplem. Figure 7a)**. We carried out immunohistochemistry assays to detect bpMOK in spinal cord tissue from a TDP-43-based mouse model (Tg^{TDP-43})[32] at the late-stage (i.e. from 16 weeks onward) and from sporadic ALS patients. Considering the significant differences in cell size measured between WT and Tg^{TDP43} samples **(Supplem. Figure 7b)**, we normalized the quantitated bpMOK levels in these samples to the cell area. Remarkably, the results revealed significantly higher levels of bpMOK in the mouse model compared to age-matched mice **(Figure 5a)**. Furthermore, assessment of bpMOK cellular signal in tissue from human subjects also showed increased bpMOK levels in ALS samples compared to age-matched controls **(Figure 5b)**.

To get an insight into MOK's possible engagement in a pathophysiological context of ALS neuroinflammation, we chose the well-established and neuroinflammation-recapitulating SOD1^{G93A} animal model[33–36], which has additionally been found to display TDP-43 functional abnormalities [37–41] and investigated the relative changes in bpMOK levels induced by LPS-stimulation in spinal cord organotypic cultures from pre-symptomatic (5-weeks old) SOD1^{G93A} mice vs. WT controls, by IF confocal analysis. As opposed to WT mice, in which no significant changes were observed when stimulated with LPS, a significant increase in nuclear bpMOK was seen in LPS-stimulated spinal cultures from ALS mice **(Figure 5c)**. Remarkably, by performing an analogous study with pBrd4 immunolabeling **(Figure 5d)** we observed that, whereas LPS stimulation resulted in upregulated nuclear pBrd4 levels in spinal cord tissue from healthy mice, no upregulation -but rather, a reduction- in pBrd4 was induced in ALS mice. These results suggest that the MOK-pBrd4 axis activated in the inflammatory response, is dysregulated in ALS.

To determine whether the levels of functional MOK kinase could be specifically altered in microglia in the context of ALS, we isolated microglial cells from spinal cord of WT or SOD1^{G93A} mice at post-onset (14 weeks) and quantified the cells displaying high levels of bpMOK among the cell population expressing the microglial surface marker CD11b, by

flow cytometry **(Figure 5e, Supplem. Figure 7c,d)**. Remarkably, bpMOK^{high} microglial cells were significantly more abundant in cells isolated from SOD1^{G93A} mice compared to controls, showing ca. 5-fold increase in the ALS model.

Finally, to investigate a possible role of MOK in the physiopathology of ALS *in vivo* and its potential as a therapeutic target, we peripherally administered the MOK inhibitor C13, or vehicle, to SOD1^{G93A} mice by intraperitoneal injection three times a week along three weeks, starting at the early onset stage (11 weeks of age; **Figure 5f)**. Assessment of motor performance by Rotarod test did not show any significant differences between both groups (**Supplem. Figure 7e**). Notably, however, C13 treatment resulted in protection during a time window at the early onset stage and reaching statistical significance one week after the end of treatment, according to relative body weight assessment, another standard parameter used to monitor disease course in this ALS model. Finally, to investigate whether the protective effects of C13 administration to SOD1^{G93A} mice might reflect suppressed microgliosis, we analysed the content of CD11b^{high} cells in spinal cord purified cells from treated or non-treated mice at week 14, i.e. at the end of treatment **(Figure 5g)**. As expected, flow cytometry analysis showed increased CD11b^{high} cell content in SOD1^{G93A} compared to WT mice, indicating increased microglia activation in ALS spinal cord[42]. Remarkably, the analysis also revealed reduced levels of CD11b^{high} in SOD1^{G93A} mice as a result of C13 administration, suggesting that MOK is indeed involved in microglial activation and neuroinflammation in the context of ALS. All together, these results demonstrate that MOK protein and its newly unleashed regulated pathways are altered in ALS spinal cord cells, including microglia, and they indicate that MOK is involved in the pathophysiology of ALS.

Discussion

Previously, we identified the Ser/Thr kinase MOK as a protein that strongly interacts with abnormal cytosolic TDP43 aggregates in microglial cells[15]. However, until now, no regulated signalling pathway or downstream molecular target has been identified for MOK, and its potential function in immune cells has not been explored. In this study we obtained a differential profile of phosphorylated protein candidates under TDP-43 aggregation conditions for C13 pre-treated cells, suggesting that MOK is regulating downstream phosphorylation events in microglia under TDP-43 aggregation, including the epigenetic reader Brd4. Furthermore, pre-treatment of microglial cells with MOK inhibitor C13 revealed a number of genes whose early expression upon exposure to TDP-43 aggregates would be

regulated by MOK, including Dtx2 (regulator of Notch signalling), Ppp5c (Ser/Thr phosphatase involved in various signalling pathways) and Sap30I (transcription repressor via interaction with histone-deacetylase complexes/HDACs). Together, these data demonstrate that MOK kinase is functionally mobilized in microglial cells under TDP-43 aggregation conditions, which suggests a role of this kinase in the pathogenic mechanisms triggered by TDP-43 aggregation processes.

By using a uniquely specific inhibitor of MOK kinase[18] and MOK-deleted cells, we showed that MOK kinase controls the inflammatory response induced by the general stimulator LPS in microglia. Moreover, by exogenous expression of recombinant WT or kinase-dead MOK protein in MOK-KO cells, we demonstrated that MOK regulates proinflammatory cytokine expression in a kinase dependent manner. By supporting IL-6, TNFα and IL-1α/β along with the activation of p65/RelA, MOK regulates the canonical inflammatory response, while also supporting IFN-β secretion and type-I IFN responses, which have been lately related to neuroinflammatory processes and disease progression in ALS and other neurodegenerative disorders[43–45]. Integrated transcriptomics analysis of enriched biological processes and KEGG pathways indicated that MOK's control of the inflammatory response in microglia is mediated by regulation of microglial activation, the 'innate immune response', IFNα/β (type-I IFN) production, and anti-viral responses. IPA prediction of upstream regulators supports that MOK mediates the 'neuroinflammation signalling pathway' in LPS-stimulated microglia by stirring the inhibition of CITED2 and TRIM24 —a critical negative regulator of inflammatory gene programs in myeloid cells [46–48] and a suppressor of type-I IFN production[49], respectively. It also predicted the activation of IRF7/3, STAT1 and BHLHE40/Dec1 upstream transcriptional regulators. IRF7/3, revealed in both RNA-seq studies with MOK-KO cells and with C13-treated primary microglia, and STAT1 are well known type-I IFN- and IL-6-promoting transcription factors, respectively [50]. MOK's support of IFN-β secretion and of the type-I IFN signature in inflammatory microglia indicate a regulation by MOK of type-I IFN response in inflammatory microglia, which has been lately related to neuroinflammatory processes in a variety of neurodegenerative situations, including ALS, Alzheimer's disease and other tauopathies, Parkinson's disease, prion-disease and traumatic brain injury[51–58]. On the other hand, BHLHE40 has been recently reported to act as a central transcription factor for pro-inflammatory gene expression in macrophages and other immune cells[59,60]. Moreover, it has been recently found to be involved in the regulation of MGnD neurodegeneration-associated microglial expression signature[36].

Remarkably, we identified the first protein whose phosphorylation state levels are physiologically regulated by MOK, the epigenetic reader Brd4. Brd4 was previously demonstrated to be phosphorylated at Ser^{492} by casein kinase II/CK2[27]. Therefore, our results indicate that MOK could possibly be acting on pBrd4 levels directly via its Ser/Thr kinase activity or indirectly, possibly by regulating CK2 activity.

Notably, Brd4 has been lately shown to play crucial roles in innate immune responses by activating transcription of a number of immune genes[21,61] and BET proteins dysfunction has been lately recently involved in various inflammation-related disorders, including cancer, neurodegenerative disease and CNS injury[21,22]. In this study, we showed that MOK supports nuclear levels of the critical phospho-Ser^{492}-Brd4 (pBrd4) state and, furthermore, we showed that MOK controls Brd4 binding to IL-6, IFNβ and TNFα gene promoters in proinflammatory microglia. This unleashed regulation of Brd4 chromatin-binding and concomitant cytokine-expression by MOK upon acute or 'non-pathological' inflammatory stimulation could be of utmost relevance as evidence toward an impact of epigenetic factors in ALS and other neurodegenerative disorders has already started to emerge[62,63] .

Finally, we showed that the levels of activated, ($Ser^{159}Tyr^{161}$)-phospho-MOK (bpMOK), either constitutive or induced by proinflammatory stimulus, are significantly altered in the spinal cord of ALS patients or animal models, indicating that MOK's physiological functions are dysregulated in the context of ALS. In particular, we reveal a massive increase of bpMOK levels in the microglia of $SOD1^{G93A}$ mice. Unexpectedly, we observed that, as opposed to WT mice, inflammatory stimulation of spinal cord samples from early pre-onset $SOD1^{G93A}$ mice fails to upregulate nuclear pBrd4 levels despite the increased expression of bpMOK, indicating dysfunctional MOK-Brd4 signalling in the ALS model. Remarkably, we observed that intraperitoneal administration of MOK inhibitor to early post-onset ALS mice results in protection from disease progression, strongly suggesting that MOK is indeed involved in ALS pathophysiology, probably by exerting different regulatory events at different stages throughout the natural history of the disease. The broad relevance of our findings is further evidenced by two recent studies revealing associations between MOK gene expression levels in peripheral leukocytes with blood pressure[64] and with type-1 diabetes[65], which supports a possible role for MOK in immune dysregulation in the context of other pathological scenarios. Indeed, protein kinases, including immune-related kinases, have been shown to play crucial roles in the physiopathology of ALS and other neurodegenerative proteinopathies and have recently emerged as attractive therapeutic targets in various neurodegenerative disorders[66,67]. Therefore, the identification of MOK-regulated proteins and

downstream signalling pathways in immune cells, particularly in the context of neuroinflammation, could set the bases for therapeutic targeting of key pathogenic pathways in ALS and other inflammation-related disorders.

Overall, we unleash a role of MOK kinase in controlling the inflammatory response in microglia via a Brd4 epigenetics-dependent mechanism and report that MOK microglial levels and its immune-related functions are dysregulated in ALS, with implications in disease physiopathology.

Methods

General reagents and DNA constructs. Lipopolysaccharide (LPS) from *Escherichia coli* (L3137, Sigma-Aldrich), (-)-JQ1 (SML1525, Sigma-Aldrich), (+)-JQ1 (SML1524, Sigma-Aldrich), polymixin B solution (81271, Merck Life Science S.L.) and dimethyl sulfoxide (DMSO, D2650, Sigma-Aldrich) were used. Compound AG2P145D/Comp13 (C13) was synthesized and characterized as previously reported[18]. Plasmids encoding FLAG-tagged MOK (murine, wild type/WT and kinase-dead/KD) were described previously[20].

Human samples. Patients spinal cord samples were obtained after voluntary donation to the Brain Bank of the Region of Murcia (BCRM) by patients diagnosed as sporadic ALS (NCT00124539, EudraCT 2006-00309612). Control spinal samples from subjects with no history of neurological diseases were donated by the BCRM. The sample collection at BCRM fulfils the ethical standards of our institution and the 1964 Helsinki declaration and its later amendments or comparable ethical standards. Prior to the spinal cord extraction, in situ exploration was performed to detect possible anatomical malformations. Transverse serial segments of 1.0 cm were embedded in paraffin, cut at 7 μm and mounted in 10 parallel series for IHC immunolabeling.

MOK-knockout cells. MOK-knockout (MOK-KO) SIM-A9 cell clones (H14 and A7) were generated by CRISPR/Cas9 technology (Synthego, Redwood City, CA, USA). Quality control of MOK-KO clones was done by Synthego. The expected mutations were confirmed by Sanger DNA sequencing (Genomics Unit, CNIO, Madrid) and clones were validated by MOK-specific qRT-PCR and Western blot by us, as shown in Supplem. Figure 2c,d.

Animal models. Spinal cord tissue slices (lumbar, sacral) for IHC studies were from late-stage Prp-TDP43^{A315T} mice (and wild-type, age-matched controls), an ALS/FTD model described previously[32]. The SOD1 mouse model was obtained from The Jackson Laboratory and the colony was maintained at the CABIMER animal facility, on a 12-hour light/dark cycle, housed at 4-8 animals/cage with constant temperature (22 °C) and humidity (60%), and with food and water available *ad libitum*. Transgenic males B6SJL-TgN(SOD1-G93A) 1Gur/J (Jackson Laboratory, No. 002726), carrying the human SOD1 gene with the G93A point mutation (SOD1^{G93A}). Genotyping to assess mutant SOD1 copy number was performed for every mouse used in experiments. At time of weaning, littermates were identified through ear punching and separated in different cages according to their gender. The ear tissue extracted during the tagging procedure was then used to run a real-time polymerase chain reaction (qPCR) for genotyping of the progeny. Animals were anesthetized intraperitoneally by injection of ketamine (100 mg/kg body weight) and xylazine (10 mg/kg body weight). Experiments followed approved Institutional animal protocols at the CABIMER institute for the care and use of laboratory animals, with ethical committee numbers 25-2010 and 02-2013 and complied with national and European Union legislation (Spanish RD 53/2013 and EU Directive 2010/63) for the protection of animals used for scientific purposes.

.

.

Administration of C13 to SOD1^{G93A} mice and weight assessment. Each mouse was injected intraperitoneally three days a week (days 1, 3 and 6) with a total of 100 µl solution consisting of 20 µg of C13 compound[18] in PBS (containing 2% DMSO) or vehicle, for a total of three weeks starting at 11 weeks of age. Mice were weighed twice a week to monitor their weight loss. Once they reached 80% of their maximum weight (considered the end-point), mice were sacrificed.

Cell culture. Mixed glial cultures were prepared from cerebral cortices of 1 day- to 3 day-old C57BL/6 male mice (University of Seville Animal Core Facility), and microglia were isolated by mild trypsinization as previously described[15]. After microglia isolation, cells were detached with acutase (A11105, Thermo Fisher Scientific) and seeded in 24-well plates at a density of 100,000 cells/mL Attached microglia were allowed to recover in conditioned medium (half new culture medium, half mixed microglia-used culture medium) for 48 h before being

subjected to different treatments. SIM-A9 microglial cell line (CRL-3265) was acquired from ATCC. SIM-A9 MOK-KO clones (and the corresponding WT control) were generated and fully characterized by Synthego (Redwood City, CA, USA) and also validated by Sanger sequencing, Western blot and qRT-PCR by us. These cell lines were maintained in DMEM-F12 (Sigma-Aldrich) that was supplemented with heat-inactivated 10% FBS and 5% HS (Gibco, Billings, MT, USA), 2 mM L-glutamine (Thermo Fisher Scientific), 100 U/ml penicillin (Thermo Fisher Scientific) and 100 μg/ml streptomycin (Thermo Fisher Scientific).

Treatment of cell cultures. Stimulation of primary or SIM-A9 microglial cultures with LPS was performed by adding one tenth volume of medium alone or containing either LPS (1 μg/mL final) and incubated for either 1, 5 or 16 h. Pre-treatment with 10 μM C13 or 10 μM (-)-JQ1/(+)-JQ1 was done in the same manner by incubating cells for 1 h prior to cell treatment. In these cases, control cultures received equal volume of DMSO. After incubation at 37°C, supernatants were harvested, clarified by mild centrifugation and stored at -20°C, and cells were either used for different purposes or frozen and stored at -20°C. For cell treatment with TDP-43 aggregates for SLAM-Seq analysis, see below.

Organotypic culture preparation and treatment. Organotypic cultures were prepared as previously described[15] from lumbar spinal cords of 5-week-old male $SOD1^{G93A}$ or wild-type (WT) mice. Cultures were maintained at 37°C in a 5% CO_2/95% air humidified environment. Cultures were left to stabilize for 4 days, then medium was changed every 3 days. After1 week, treatments were performed by adding one tenth volume of fresh medium containing LPS (1 μg/mL final) or medium alone. After overnight incubation, supernatants were harvested and significantly upregulated IL-6 cytokine levels were confirmed by ELISA in all LPS-treated cultures as a stimulation check-up. In addition, organotypic cultures were processed for immunofluorescence analyses (see below).

Acute microglial cell isolation from adult mice. Microglial cells from adult mice were acutely isolated from spinal cord tissues of 14 weeks old $mSOD1^{G93A}$ Tg mice and their WT littermates. Mice were anesthetized by intraperitoneal injection of a Ketamine/Xylazine mixture, and intracardially perfused with phosphate-buffer saline (PBS). Spinal cords were extracted by flushing the spinal canal with PBS and minced into 2-3 mm pieces with a disposable scalpel in ice-cold Hank´s-balanced salt solutions (HBSS, cat. 14170-088). Each

spinal cord microglial preparation was derived from a single animal by enzymatic digestion and mechanical disruption, and separation by density gradient, as detailed. Spinal cord fragments were dissociated with 0.25 % trypsin-EDTA for 10 min at 37 °C (GIBCO, cat. 25200072). Then trypsin treatment was stopped by adding RPMI 1640 medium (Sigma, cat. R8758) with 10% (v/v) FBS. The spinal fragments were then mechanically dissociated by repeated pipetting and by passing through a 70 µm cell strainer (Falcon cat. 352350s). Microglia was further purified for myelin removal by using Percoll gradient. Cells were collected by centrifugation at 350g for 10 min at 4 °C, the cell pellet resuspended in 2 ml of 70% isotonic Percoll, and then carefully over layered with 3 mL of 35% Percoll in PBS, and 2 ml of PBS. The discontinuous gradients were centrifuged at 850 g for 35 min at room temperature. The upper layer containing the white in appearance myelin debris was then removed. Cells were isolated from the gradient interface, washed in three volumes of PBS by centrifugation at 500 g for 5 min, and resuspended in RPMI 1640 medium supplemented with 2% FBS for cell counting and flow cytometry analysis.

Immunolabeling of acutely isolated microglial cells and flow cytometry analysis

Cells were stained on ice for 30 min with rat anti-Cd11b-APC (BD Biosciences, cat. 553312) or appropriate antibody isotype controls Rat Anti-Mouse IgG1-PE (BD Biosciences, cat. 562027), diluted in PBS with 1% FBS and 1mM sodium azide. For intracellular labelling of bi-phosphorylated MOK protein (bpMOK), cells were fixed and permeabilized with the Cytofix/Cytoperm Plus Fixation/Permeabilization Kit (BD Biosciences, cat. 554722) according to the manufacturer instructions and stained with anti-MOK antibody bi-phosphorylated (pThr159+pTyr161, StressMarq, cat. SPC-1030), followed by donkey anti-rabbit IgG-Alexa Fluor 488 (Invitrogen, cat. A-21206). Antibodies for intracellular labelling were diluted in Perm/wash Buffer (BD Biosciences, cat. 554723). Samples were analysed using a FACSCalibur (BD Biosciences, Madrid, Spain). To discriminate between living and dead cells, cells were acquired in presence of propidium iodide, and dead cells were excluded from gates. Data were analysed using either Cell Quest Software (Becton Dickinson, Mountain View, CA, USA) or the WinMDI 2.8 software (from http://www.cyto.purdue.edu/flowcyt/software/Winmdi.htm).

Immunohistochemistry (IHC) and IHC analyses. IHC assays and quantification were double blinded. Fixed spinal cord segments from Tg^{TDP-43} and control mice and controls (lumbar region) or human sporadic ALS patients (with no known mutations, lower thoracic

or higher lumbar region and obtained as explained before), were embedded in paraffin and sectioned to 10 µm-thick slices. After deparaffinization, sections were incubated with 1x citrate buffer (Sigma Aldrich, St. Louis, MO, USA) for 30 min at 95 ºC for antigen retrieval, followed by incubation in 3% (w/v) H_2O_2 to inhibit endogenous peroxidase activity. Sections were then incubated with 1% Bovine Serum Albumin (BSA) blocking solution for 1 h at room temperature, followed by overnight incubation at 4 ºC with primary antibodies (see Tables I and II for antibody information). Then, sections were washed and incubated with the appropriate secondary biotinylated antibodies, followed by incubation with the avidin-biotin complex (Vectastain ABC-HRP Kit, Peroxidase-Rabbit IgG; Vector Laboratories, USA). Finally, sections were treated with diaminobenzidine-nickel substrate (DAB-nickel; Vector Laboratories) and then examined under a Leica DM6000B microscope. Images were acquired at 40x magnification. For comparative signal quantification, cell size and signal intensity for at least 50 cells (with visible nucleus on the plane) from three or four different, non-overlapping fields were assessed for each sample (corresponding to each individual; N=3/experimental group) with the Fiji software (OpenSource). The background intensity -determined from 5 regions from 4 different images- was subtracted from the calculated signal intensities. In human samples, the less abundant very large cells (>2000 pixels, corresponding to >110 μ^2) were excluded from the analysis. The mean intensity per cell and the intensity per cell area were calculated from all analysed cells for each sample/individual.

Immunofluorescence (IF) of cultured cells. For IF analyses, SIM-A9 cells or highly pure primary microglial cultures obtained as described above were used. Primary cell cultures were seeded on pre-treated poly-D-Lys (Sigma-Aldrich) glass lamellas. For the immunolabeling step, treated microglial cultures were fixed in cold PBS that contained 4% paraformaldehyde (Sigma-Aldrich) for 20 min at 4°C. After washing with PBS, cells were incubated with PBS that contained 0.5% (v/v) Triton X-100 (Sigma-Aldrich) and 3% bovine serum albumin (Sigma-Aldrich) for 1 h at 4 °C, for blocking and permeabilization. Cells were incubated overnight at 4 °C with Phospho-Brd4 (Millipore, Cat. ABE1451) primary antibodies (1:500). After washing with PBS, cells were incubated for 1 h at room temperature with their corresponding conjugated secondary antibodies, which were Alexa-Fluor488 donkey anti-rabbit IgG (Thermo Fisher, Cat. A-21206) (1:1000). After washes with PBS, nuclei were counterstained by incubating cells with PBS that contained 1 µg/mL DAPI (Sigma-Aldrich, Cat. D9542) for 15 min at room temperature. Fluorescence images were captured with

automated upright microscope (Confocal Lase Scanning Microscope TCS SP5; Leica Microsystems. Images were taken at 63x magnification from randomly chosen fields.

Immunofluorescence (IF) of organotypic slices. Following treatment with LPS (or medium alone), spinal cord slices were fixed with 4% paraformaldehyde in PBS for 3 h at 4 °C. After blocking with 5% normal donkey serum (Merck Millipore) and 0.5% (v/v) Triton X-100 in PBS, sections were incubated with anti-bpMOK or anti-pBrd4 antibodies from rabbit. Slices were thoroughly washed in PBS with 0.2% Tween-20 and incubated with Alexa-Fluor 488-labeled donkey anti-rabbit IgG secondary antibody (1:1000; Thermo Fisher Scientific) diluted in PBS with 0.1% Triton X-100 and 1% of normal donkey serum for 2 h at room temperature. Finally, cell nuclei were labelled with 1 μg/ml DAPI for 15 min in PBS and sections were mounted with Vectashield medium (Vector Laboratories, Burlingame, CA, USA). Slices were analysed under confocal microscope (Confocal Laser Scanning Microscope TCS SP5; Leica Microsystems).

Cytokines determination by ELISA. Primary microglia or SIM-A9 cell cultures were stimulated as described before. Harvested culture supernatants were centrifuged at 400 g for 5 min, and cell-cleared supernatants were recovered and stored at -20 °C before cytokine measurement. IL-6 and TNF-α levels were assayed with Mouse IL-6 or TNF-α BD OptEIA ELISA set (BD Biosciences, Cat. 555240 and 555268, respectively). IFN-β and IL-1α were assayed with Mouse IFN-β and IL-1α/IL-1F1 DuoSet ELISA kits (R&D Systems, Cat. DY8234 and DY400, respectively). All cytokine quantifications were done by following the manufacturer's protocol.

Transfection of microglial cell cultures. For the overexpression of FLAG-tagged WT-MOK and KD-MOK constructs, Glial Mag transfection reagent (OzBiosciences, Cat. KGL0250) was used. The protocol was carried out according to manufacturer's instructions. Plasmids were diluted in Optimem medium (Gibco, Cat. 31985062), and 1 μL of Glial Mag and 0.5 μg of plasmid were employed, and volumes and concentrations were optimized for a 24-well plate assay. Transfection time was of 30 h in total, including a 6 h-stimulation with/without 1μg/mL LPS and GolgiStop (BD Biosciences, Cat. 554724).

Immunolabelling and Flow Cytometry of transfected cells. Cells were fixed and permeabilized for 20 min at 4 ºC by using Fixation/Permeabilization solution (BD Biosciences, Cat. 555028). After washing twice with Wash Buffer (2 mM EDTA, 2% v/v FBS in PBS), cells were incubated for 15 min at room temperature in Perm/Wash Buffer (BD Biosciences, Cat. 555028). Immunostaining was performed using APC-conjugated anti-FLAG (Abcam, Cat. Ab72569) and PE-conjugated anti-IL-6 (BD Biosciences, Cat. AB395367) at a 1:40 dilution in both cases in Perm/Wash Buffer, and incubated at 4 ºC in the dark for 30 min After antibody incubation, cells were washed twice with Perm/Wash Buffer and resuspended in Wash Buffer, and were kept at 4 ºC in the dark until analyses with LSR Fortessa X-20 cytometer (BD Biosciences).

Preparation of cell lysates. Cells were cultured in 12-well plates at 400,000 cells/mL for 24 h previous to treatment. After treating as required, cells were washed with cold PBS and lysed in lysis buffer (50 mM Tris pH 7.4, 150 mM NaCl, 0.25% deoxycholate, 10% glycerol, 0.1% SDS, 0.01% IGEPAL) containing Complete EDTA-free Protease inhibitor cocktail tablets (Roche, Cat. 11836170001), 1 mM PMSF (ITW Reagents, Cat. A0999) and PhosSTOP (Roche, Cat. 04906845001). Lysates were incubated for 5 min at 37 ºC followed by a 20 min incubation in ice with manual agitation every 5 min They were then centrifuged at 12,000 g for 5 min at 4 °C. Cleared supernatants were collected and stored at -20 °C until use. Protein concentration was determined using Micro BCA™ Protein Assay Kit (Thermo Fisher, Cat. 23235), following manufacturer's instructions.

Western Blot assays. Equal volumes of cell lysate (20 µl) with comparable protein content (40-50 µg) were subjected to 10% or 12% SDS-PAGE electrophoresis and semi-dry or wet transfer to a 0.2 µm nitrocellulose or PVDF membrane (Amersham, Cat. 10600006 and Amersham, Cat. 10600021, respectively). After blocking with 5% (w/v) non-fat milk in Tris-buffered saline with 0.05% Tween 20 (TBST) during 1h at room temperature (RT) and washings with TBST, membranes were incubated overnight at 4 ºC with the corresponding primary antibodies against: (Ser492) Phospho-Brd4 (Millipore, Cat. ABE1451) (1:500), Brd4 (Bethyl, Cat. A301-985A100) (1:1000), MOK (Abbexa, Cat. abx129598) (1:1000), Ser536-Phospho-NFκB p65 (ThermoScientific, Cat. PA5-17782) (1:1000), p65 (Cell Signalling, Cat. 3034) (1:1000). The following day membranes were washed with TBST and incubated with the appropriate HRP-conjugated secondary antibody: goat anti-mouse IgG (Pierce, Cat. 32430) (1:2500) or goat anti-rabbit IgG (Pierce, Cat 31460) (1:10000), for 1 h at room

temperature. Finally, after washings with TBST, the substrate solution ECL reagent (Merck Millipore, Cat. WBKLS0500) was added and bands were detected using a ChemiDoc™ MP Imaging System (Bio-Rad, Cat. 1708280). The results were quantified using the ImageLab Software 6.1 and normalized against the housekeeping gene GAPDH (Millipore, Cat. MAB-374) (1:2500) or α-tubulin (Sigma-Aldrich, Cat. T6199) (1:6500), accordingly.

Preparation of TDP-43 aggregates. TDP-43 and sham aggregates were obtained by purifying the inclusion body fraction after overexpression of His_6-human TDP-43 fusion protein (by using a plasmid construct kindly provided by Yoshiaki Furukawa's laboratory, Keio University, Yokohama, Japan) in *E. coli* BL21(DE3) cells, or empty vector, as previously described[15]. General characterization of the *in vitro*-prepared TDP-43 aggregates was done as before[15].

Cell culture treatment and cell lysate preparation for anti-phospho-Ser/Thr IP assays. Primary microglial cells in culture were pre-treated with 10 μM final C13 or DMSO for 1 h and then to 5 μg/mL TDP-43 or sham aggregates in medium containing polymyxin B (10 μg/mL). Following two washes with PBS, cells were lysed with NP-40 lysis buffer (Invitrogen, FNN0021) supplemented with protease inhibitors cocktail (Roche), 1 mM PMSF (ITW Reagents, Cat. A0999) and PhosSTOP (Roche, Cat. 04906845001). For the IP procedure, Protein A Dynabeads (Invitrogen, 10001D) were used. After incubating the beads with 2 μg of anti-phospho-Ser/Thr rabbit antibody (Abcam, Cat. ab17464) for 1h at room temperature under rotation, crosslinking of the captured antibody was performed with BS3 (Thermo Fisher, Cat. 21580) according to the manufacturer's protocol. Afterwards, the beads-antibody conjugates were added to the cell lysates and incubated for 1 h at room temperature under rotation. After washing, elution was carried out with 50 mM glycine solution (pH 2.8) and the eluate was pH-equilibrated with PBS for subsequent LC-MS/MS analysis.

LC-MS/MS and protein identification. IP protein eluates were subjected to TCA/acetone precipitation and the pellet was resuspended in a solution of 0.2% RapiGest in 50 mM ammonium bicarbonate. DTT was added to 5 mM final concentration and incubated for 30 min at 60 ºC. Afterwards, chloroacetamide was added to 10 mM final concentration and incubated for 30 min at room temperature in the dark. Trypsin digestion was done overnight at 37 ºC at a 1:40 (trypsin:protein) ratio. The next day, trypsin was inactivated with formic

acid and acetonitrile was added to a final concentration of 2%. Injection volume was 10 µL per run.

LC-MS/MS analyses were done in a TOF (5600 Plus, Sciex) triple quadrupole equipped with a nano electrospray source coupled to a nanoHPLC Eksigent. Analyst TF 1.7 software was used for control of equipment and for the acquisition and processing of data. Peptides were first loaded in a 'trap column' (Acclaim PepMap 100 C18, 5 µm, 100 Å, 100 µm id × 20 mm, Thermo Fisher Scientific) in an isocratic manner in 0.1% formic acid/2% acetonitrile (V/V) at a 3 µL/min flow for 10 min Then, they were eluted in a reverse-phase analytical column (Acclaim PepMap 100 C18, 3 µm, 100 Å, 75 µm id × 150 mm, Thermo Fisher Scientific) coupled to a 'PicoTip emitter' (F360-20-10-N-20_C12, New Objective). Peptides were eluted with a linear gradient of 2-35 % (v/v) solvent B in 60 min at a 300 nL/min flow. Solvents A and B were 0.1% formic acid (v/v) and acetonitrile with 0.1% formic acid (v/v), respectively. Source voltage was selected at 2600 V and heater temperature was maintained at 100 ºC. Gas 1 was selected at 15 psi, gas 2 at zero, and curtain gas at 25 psi. For protein identification, acquisition was carried out with a Data Dependent Acquisition (DDA) method consisting of a TOF-MS with a sweep window of 400-1250 m/z, accumulation time of 250 ms, flowed by 50 MS/MS with a sweep window of 230-1500 m/z, accumulation time of 65 ms and a total cycle time of 3.54 s.

For protein identification, the ProteinPilot v5.0.1 (Sciex) software was used with a Paragon method, with trypsin as the enzyme and iodoacetamide (IAA) as the Cys alchylating agent, using the reference proteome of mouse (*mus musculus*) downloaded from uniprot.org (02/2021) in a FASTA format as the databank, fused with the Sciex contaminants. A false-positives analysis was done and proteins with FDR (False Discovery Rate) lower than 1% were selected.

RNA isolation and cDNA synthesis for qRT-PCR. Total RNA from SIM-A9 or primary microglial cells was extracted by using Primezol (Canvax, Cat. AN1100). Cells were directly lysed in 12-well culture plates by adding 1 mL of Primezol per well. Samples were incubated 5 min at room temperature and then 200 µL of chloroform was added. Tubes were shaken vigorously by hand for 15 sec. and incubated 3 min at room temperature and then centrifuged at 12000 g for 15 min at 4 ºC. The upper layer containing RNA was separated and transferred into a new tube without disturbing the interphase. RNA was precipitated by adding 0.5 mL of isopropyl alcohol and incubated for 10 min at room temperature. Tubes were centrifuged again at 12000 g for 10 min at 4 ºC. Supernatant was removed and pellet was washed once with

70% ethanol. Finally, tubes were centrifuged at 7500 g for 5 min at 4 ºC. Supernatant was removed once more and pellet was air-dried. Pellet was dissolved in RNAse-free water and stored at -80 ºC. After extraction, 1 µg of RNA was reverse-transcribed by using PrimeScript RT reagent Kit (Takara, Cat. RR047Q) following the manufacturer's guidelines.

qRT-PCR. Quantitative real-time PCR (qRT-PCR) with template cDNA was performed by using iTaq Universal SYBR Green Supermix (Bio-Rad, Cat. 1725124) on a QuantStudio 5 Real-Time PCR System. Primers pairs (Sigma-Aldrich) were preferentially designed or selected to anneal in different exons and they were as follows: MOK, HPRT, IL-6, IFNβ, TNFα, IL-1α, IRF7 (Table III). Amplicons were analysed for 40 cycles by using an optimized qRT-PCR thermal profile. Changes in gene expression were determined by applying the formula $2^{-\Delta\Delta Ct}$ where ΔCt is calculated taking HPRT as endogenous control. ΔΔCt values were calculated by subtracting the average ΔCt values obtained for non-treated cell samples.

RNA-Seq analyses. RNA-Seq analyses were carried out by the Genomics Unit, CABIMER (Andalusian Center for Molecular Biology and Regenerative Medicine, Seville, Spain). For transcriptional analyses of MOK-KO vs. WT SIM-A9 cells, total RNA-Seq was used. After removing the culture supernatant, cells were washed twice with PBS and RNA was extracted using the RNeasy Mini Kit (Qiagen, 74104) according to the manufacturer's guidelines. RNA samples were quantified using Qubit RNA HS Assay Kit and RNA size profile and integrity were analysed on Bioanalyzer 2100 (Agilent). RNA quality was considered 'excellent' and RNA integrity number estimates for all samples were between 9.7 and 10.0. After ribosomal RNA depletion, strand-specific (cDNA) libraries preparation was performed by applying Stranded TOTAL RNA prep Ligation with RIBO-ZERO PLUS kit (Illumina), following the manufacturer's instructions. Adapters (Illumina) included a sample/library-specific index. After library amplification by PCR and all recommended quality control assays, libraries were normalised using Qubit and quality control was performed with Bioanalyzer 2100. Individual libraries were pooled together at equimolar ratios and diluted to ~1.2 nM. Pooled libraries were denatured and further diluted prior to loading on the sequencer. Paired-end sequencing was performed using a NovaSeq6000 SP and 2x50bp (Illumina), generating a raw read count of >68 million reads per sample. Sequencing quality as assessed with BaseSpace Hub software (Illumina) was high (89.8% >Q30 and >106 Gb depth).

For mRNA-Seq transcriptional analyses from primary microglial cells, sequencing of mRNA was carried out. The procedure was as described above, with the following changes:

mRNA was isolated by using poly-dT-coated beads and libraries were prepared by the TruSeq Stranded mRNA kit (Illumina). After library amplification by PCR and all recommended quality control assays, individual libraries were pooled together at equimolar ratios and diluted to ~1.4 pM. Paired-end sequencing was performed using NextSeq 500 Mid Output and 2x75pb (Illumina), generating a raw read count of >24 million reads per sample. Sequencing quality as assessed with BaseSpace Onsite software (v. 3.22.91.158, Illumina) was high (88% >Q30 and >24 Gb depth).

RNA-Seq and mRNA-Seq data processing. RNA-Seq sequencing data were generated from four cell treatments with three biological replicates each (12 samples in total), by using the paired end approach of Illumina technique. Total paired end fastq files were used for the RNA-Seq analysis via the pipeline: FastQC-Trimmomatic-STAR-FeatureCounts-DESeq2. STAR aligner (v. 2.7.9a) was used to perform read alignment and mapping to the reference genome, the latest release of the mouse genome from Ensembl (*mus musculus*) genome database. The feature Counts module of R-package Rsubread (v. 2.0.1) was used for extracting raw read counts for all the samples. These raw read counts were then used to perform the differential expression analysis by using the DESeq2 package (v. 1.32.0) in R.

mRNA-Seq sequencing data were generated from two cell treatments with three biological replicates each (6 samples in total) as described above, with the following changes: Fastq files were generated with the pipeline FASTQ Toolkit (v1.0.0, Illumina) with filtering, timming and de-multiplexing data. The reference genome was Mus musculus (UCSC mm10). Cufflinks Assembly & DE, BaseSpace Workflow (v. 2.1.0, Illumina) was used to perform the differential expression analysis.

Gene set enrichment analysis and ingenuity pathway analysis (IPA). Gene Ontology (GO) and Pathway Enrichment Analysis. For each comparison group of SIM-A9 cells (WT Ctrl, WT+LPS, MOK-KO Ctrl, MOK-KO+LPS), gene ontology and pathway enrichment analyses were performed using the R-package PathfindR (v1.6.2). All differentially expressed genes (DEGs) obtained after applying the filter on Log2 Fold Change values >2 or <-2 along with P value <0.05 were used as input to perform enrichment for the following categories: GO Biological Process, GO Cellular Component, GO Molecular Function and KEGG Pathway. Ingenuity Pathway Analysis was applied on DEGs as defined above.

S4U-labeling and SLAM-Seq analysis. After pre-treatment with 10 μg/mL polymixin B, SIM-A9 cells in culture were incubated with 10 μg/mL C13 (or DMSO) for 1 h. Then, one tenth volume of medium without serum containing TDP-43 or sham aggregates (5 μg/mL final) were added to each well and incubated for 2.5 hours. This was followed by addition of 4-thiouridine (S4U, Cayman Chemical 16373) to a final concentration of 100 μM (found by us to retain 80% of cells viability by MTT assay after 2 h) and incubation for a further 90 min in the dark. After washing with PBS, total RNA was extracted with easy-BLUE (iNtRON Biotechnology) and protected from light during the procedure to prevent S-S cross-binding. 5 μg of RNA was used for SLAM-seq modifications, as described in[68]. Briefly, iodoacetamide (Sigma I1149) was conjugated to 4SU in a 50 mM pH 8.0 phosphate buffer in DMSO/Water (1:1), the reaction was quenched with DTT and RNA was reprecipitated using ethanol and NaOAc. Libraries were prepared using Quantseq 3' mRNA-Seq Library Prep Kit (Lexogen). SLAM-Seq analysis was done similar to previously reported[69].

Chromatin immunoprecipitation (ChIP) and ChIP-qPCR. SIM-A9 cell cultures were crosslinked with 1% (v/v) formaldehyde in crosslinking buffer (50 mM Hepes pH 8.0, 0.1 M NaCl, 0.1 mM EDTA pH 8.0, 0.5 mM EGTA pH 8.0). After 10 min of incubation at 37ºC, the crosslinking reaction was stopped with 125 mM glycine for 5 min at room temperature. After washing twice with cold PBS, cells were collected by scraping in PBS supplemented with Protease inhibitor cocktail (PIC, Sigma-Aldrich, Cat. 11836170001) and PMSF (ITW Reagents, Cat. A0999). Cells were lysed by consecutively resuspending the pellet in two different lysis buffers (5mM PIPES pH 8.0, 85 mM KCl, 0.5% IGEPAL and PIC, and 1% SDS, 10 mM EDTA pH 8.0, 50 mM Tris-HCl pH 8.1 and PIC) with a centrifugation step in between. Lysates were sonicated with Digital Sonifier 450 (BRANSON) to obtain chromatin fragments of 200-500 bp. Samples were incubated with anti-BRD4 antibody (Bethyl) and retrieved with Protein G-Dynabeads (Thermo Fisher, Cat. 1004D). After the cross-linking was reversed, chromatin fragments were treated with proteinase K. DNA fragments were purified using a ChIP DNA Clean & Concentrator Kit (Zymo Research, Cat. D5205). qPCR was performed as described above. In order to analyze the qPCR data of immunoprecipitated samples, normalization to the input DNA was performed. Primers pairs (Sigma-Aldrich) specific for IL-6 TNFα and IFNβ promoters were designed to define an amplicon of 100-170 bp (Table III).

Statistical analyses. Data are presented as mean ± SEM. Statistical analyses were performed using either One-way ANOVA followed by Tukey's post-hoc test or Student's t-test in the GraphPad Prism software, two-/one-tailed as indicated in the corresponding figure legend. P values less than or equal to 0.05 were considered statistically significant. Statistical analyses were performed using the GraphPad Prism software v.8 (GraphPad Software, La Jolla, USA).

Table I. List of primary antibodies used

Antibodies	Host	Manufacturer	Catalog number	Application
MOK	Rabbit	Abbexa	abx027945	IHC, WB
MOK (pT159+pY161) (bpMOK)	Rabbit	StressMarq Biosciences	SPC-1030	IF, Flow cytom.
Phospho-Ser/Thr	Rabbit	Abcam	ab17464	IP
Brd4	Rabbit	Bethyl	A301-985A100	ChIP
Phospho Brd4 (Ser492)	Rabbit	Millipore	ABE1451	IF, WB
Non-immune IgG	Rabbit	Sigma-Aldrich	I5006	ChIP, Co-IP
FLAG, APC-conjugated	Mouse	Abcam	ab72569	Flow cytom.
IL-6, PE-conjugated	Rat	BD Biosciences	AB_395367	Flow cytom.
TNFα, Alexa-Fluor^{488}-conjugated	Rat	BD Biosciences	AB_396828	Flow cytom.
p65	Rabbit	Cell Signaling	Cat. 3034	WB
p-p65	Rabbit	Thermo Scientific	Cat. PA5-17782	WB
CD11b	Rat	Abcam	ab8878	Flow cytom.
	Rat	Novus Biologicals	NBP1-45013	Flow cytom.
Caspase-1	Mouse	Adipogen	AG-20B-0042-C100	WB
GAPDH	Mouse	Millipore	MAB-374	WB
α-tubulin	Mouse	Sigma-Aldrich	T6199	WB

Table II. List of secondary antibodies used

Antibodies	Host	Manufacturer	Catalog number	Application
Anti-rabbit IgG, HRP conjugated	Goat	Thermo Scientific (Pierce)	31460 (1858415)	WB
Anti-mouse IgG, HRP conjugated	Goat	Thermo Scientific (Pierce)	32430 (1858413)	WB
Anti-rabbit IgG, Alexa- Fluor488	Donkey	Thermo Fisher	cat. A-21206	IF

Table III. List of PCR primers used

Primer name	Direction	Primer sequence
MOK	For	5'-GTTCTACGAGATTGCCAGCCT -3'
	Rev	5'-CTGCTTTCTGCCTTCCTGTGAGA -3'
HPRT	For	5'-GGACTAATTATGGACAGGACTG -3'
	Rev	5'-TCCAGCAGGTCAGCAAAGAA -3'
IL-6	For	5'-TCCGGAGAGGAGACTTCACA -3'
	Rev	5'-TTCTGCAAGTGCATCATCGT -3'
TNFα	For	5'-GCCTCTTCTCATTCCTGCTTG -3'
	Rev	5'-CTGATGAGAGGGAGGCCATT -3'
IFNβ	For	5'-CCACCAGCAGACAGTGTTTC -3'
	Rev	5'-GAAGATCTCTGCTCGGACCA -3'
IL-1α	For	5'-CGAAGACTACAGTTCTGCCATT -3'
	Rev	5'-GACGTTTCAGAGGTTCTCAGAG -3'
IRF7	For	5'-GGTCGTAGGGATCTGGATGA -3'
	Rev	5'-ACCTTATGCGGATCAACTGG -3'
IL6 prom. [28]	For	5'-TGTGGGATTTTCCCATGAGT -3'
	Rev	5'-TGCCTTCACTTACTTGCAGAGA -3'
TNFα prom. [70]	For	5'-GGACTAGCCAGGAGGGAGAA -3'
	Rev	5'-TGTCTTTTCTGGAGGGAGATGT -3'
IFNβ prom. [71]	For	5'-GCCAGGAGCTTGAATAAAATG -3'
	Rev	5'-CTGTCAAAGGCTGCAGTGAG -3'

Acknowledgments
We are very grateful to Prof. Kevan Shokat and Dr. Flora Rutaganira, University of California, San Francisco (UCSF, San Francisco, USA) for kindly supplying us with C13 compound. Financial support to C.R. was provided by the Spanish Ministry of Economy (RTI2018-098432-B-I00), Fundación Ramón Areces (CIVP19A5938), the Andalusian Regional Government-FEDER (US-1265227) and I+D PAIDI (PY20_01097). V.C-G. is supported by the Institute of Health Carlos III, Spain, co-funded by the European Social Fund (CP19/00046). S.M. was supported by Generalitat Valenciana (GVA: Prometeo/2018/041 and CIPROM/2021/018); MINECO/AEI/ERDF, EU, the Spanish Ministry of Economy, Industry and Competitiveness, the Spanish State Research Agency co-funded by ERDF (PID2020-118171RB-100); and Instituto de Salud Carlos III (RD16/001/0010, co-funded by ERDF).

Figure legends

Figure 1. MOK-mediated mechanisms occur in microglial cells upon exposure to TDP-43 aggregates. a) Venn diagrams showing the number of DEGs from analyzed SLAM-Seq data obtained with SIM-A9 cells exposed to 5 μg/mL TDP-43 aggregates (TDP43) or sham aggregates (Sham) for 4 h, pre-treated for 1 h with 10 μM C13 (or DMSO as vehicle). Results are from three independent experiments (N=3). Indicated are the number of DEGs for 'C13-Sham vs. Sham' and 'C13-TDP43 vs. TDP43' comparisons (pAdj.<0.05). **b)** Predicted network analysis based on the two sets of identified DEGs by using GeneMANIA[19]. Blue labels correspond to top DEGs and red labels, to inferred genes. **c)** Heatmap representing the relative expression profiles (DEGs with pAdj.<0.05) comparing 'TDP43 vs. Sham' and 'C13-TDP43 vs. TDP43' treatments. The differential regulation in gene expression changes between both comparisons indicates an effect of MOK inhibitor C13 in transcriptional profile of microglial cells upon exposure to TDP-43 aggregates. **d)** Schematic representation of LC-MS/MS analysis of eluates from anti-phospho-Ser/Thr immunoprecipitation assays of lysates from primary microglial cells exposed to 5 μg/mL TDP-43 aggregates, pre-treated for 1 h with 10 μM C13 (or DMSO as vehicle).

Figure 2. MOK positively regulates microglial responses, including inflammatory and type-I IFN pathways. a) Quantification of pro-inflammatory cytokines by ELISA in supernatants from primary microglial cells stimulated with 1 μg/mL LPS for 5 h (TNFα) or 24 h (IL-6, IL-1β) after pre-treatment with 10 μM C13 (or DMSO) for 1 h (N=4). One-way ANOVA followed by Tukey post-hoc test. **b)** Top predicted upstream regulators by Ingenuity Pathway Analysis (IPA) from 158 DEGs (C13-treated vs. untreated, pAdj<0.05) identified by RNA-Seq studies from primary microglial cells stimulated with 1 μg/mL LPS for 5 h. The P-values of overlap are shown in parentheses. **c)** Assessment of gene expression levels for a set of key cytokines by qRT-PCR from WT and MOK-KO SIM-A9 cells stimulated with 1 μg/mL LPS for 5 h (N=3). Data represent fold-changes relative to unstimulated WT cells (values were 1 or lower for unstimulated WT and MOK-KO controls; not shown). $^{\#}$P<0.05, $^{\#\#}$P<0.01 and $^{\#\#\#}$P<0.001 vs. unstimulated controls. One-way ANOVA followed by Tukey post-hoc test. **d)** Quantification of TNFα, IL-6, IFNβ and IL-1α levels by ELISA in supernatants from WT and MOK-KO SIM-A9 cells stimulated with 1 μg/mL LPS for 5 h or overnight for IL-1α (N=5 for IL-6, TNFα and N=4 for IFNβ, IL-1α). One-way ANOVA followed by Tukey post-hoc test. **e)** Flow cytometry analysis IL-6^{+} cells in WT and MOK-KO SIM-A9 cells, previously stimulated with 1 μg/mL LPS for 5 h (left). Rescue of phenotype in MOK-KO cells resulting from cell transfection with FLAG-MOK-WT or FLAG-MOK-KD constructs and stimulation with 1 μg/mL LPS for 5 h (right) (N=3). One-way ANOVA followed by Tukey post-hoc test. **f)** Fold-changes of primary motor neurons (MNs) survival (relative to each control) after exposure to conditioned media from LPS-stimulated WT and MOK-KO cells (N=3). Student's t test performed between shown groups, unpaired, two-tailed. Data in **a, b, d-f** are the mean -/+ S.E.M. from 'N' independent experiments, and *P<0.05, **P<0.01 and ***P<0.001. NS: not significant.

Figure 3. Transcriptomic analysis from RNA-Seq studies of MOK-KO cells and response to LPS stimulation. Data in **a-e** are from 3 independent experiments (N=3). **a)** Venn diagrams depicting the number of total (top) and protein-coding (bottom) DEGs between MOK-KO and WT SIM-A9 cells under basal conditions and/or after 1 μg/mL LPS stimulation for 5 h (pAdj.

<0.05; log2 fold-change>2 and <-2); **b)** Heatmap showing unsupervised clustering analysis for the top 100 protein-coding genes based on relative expression levels in the four samples; **c)** GO 'biological process' term enrichment analysis of total DEGs for MOK-KO+LPS vs. WT+LPS. Shown are the top hits based on p-value (indicated in parenthesis) with at least three up/downregulated genes; **d)** Heatmap depicting clustering analysis for 100 coding DEGs identified for the MOK-KO+LPS vs. WT+LPS comparison (consisting of the top 80% downregulated and top 20% upregulated, genes to maintain proportionality of all significant DEGs found); **e)** Top-10 IPA-predicted upstream expression regulators from all coding DEGs comparing MOK-KO vs. WT cells upon LPS stimulation, indicating positive (activated) or negative (inhibited) z-scores. The results are from all genes that were found to be misregulated in the RNA-Seq deseq2 analysis in any comparison with pAdj of <e-5. The P-value of overlap is indicated in parentheses; **f)** Assessment of IRF7 gene expression by qRT-PCR from WT and MOK-KO SIM-A9 cells stimulated with 1 μg/mL LPS for 5 h. Data represent fold-changes relative to unstimulated WT cells (WT Ctrl) (N=4). One-way ANOVA followed by Tukey post-hoc test. Data are the mean -/+ S.E.M. from N independent experiments, and *P<0.05 and **P<0.01.

Figure 4. MOK regulates phospho-Ser^{492}-Brd4 levels under neuroinflammatory conditions. a,b) Quantification of nuclear pBrd4 levels by confocal IF with anti-pBrd4 (green) and DAPI staining of primary microglial cells pre-treated with 10 μM C13 (or DMSO) for 1 h and stimulated or not with 1 μg/mL LPS for 4 h. The data and images shown correspond to one experiment (N=20 analyzed images per condition) and are representative of two independent experiments. Scale bar: 10 μm. Student's t-test (between two groups as indicated), unpaired, one-tailed. **c,d)** Quantification **(c)** and representative image **(d)** of Western blot analyses with anti-pBrd4 and anti-Brd4 (normalized to Brd4 or α-tubulin signal, respectively) in lysates of WT and MOK-KO SIM-A9 cells stimulated with 1 μg/mL LPS for 1 h. Data are from three independent experiments (N=3). Student's t-test, unpaired, one-tailed. **e,f)** Quantification **(e)** and representative images **(f)** of confocal IF analyses of nuclear pBrd4 levels with anti-pBrd4 (green) and DAPI staining of WT and MOK-KO SIM-A9 cells stimulated or not with 1 μg/mL LPS for 1 h. Signal was enhanced by 50% in all four images in the first row for better visualization. Images are from one out of three independent experiments (N=3). Scale bar: 10 μm. Student's t-test, unpaired, two-tailed. **g)** ChIP-PCR assessment of Brd4-binding to specific cytokine promoters. Represented data are relative values (percentage of input) of PCR products for IL-6, IFNβ and TNFα promoters after ChIP assay with either anti-Brd4 or IgG control antibodies with chromatin isolated from WT or MOK-KO cells treated or not with 1 μg/mL of LPS for 1 hour (N=4). Student's t-test, paired, one-tailed. Data are the mean -/+ S.E.M. from 'N' independent experiments, and *P<0.05, **P<0.01 and ***P<0.001. NS: not significant.

Figure 5. MOK is altered in CNS cells in the context of ALS. Quantification of bpMOK levels by IHC analysis in spinal cord tissue samples (left) and representative IHC images (right) for spinal tissue samples from **a)** sporadic ALS patients and age-matched control subjects (N=4), **b)** and Prp-TDP43^{A315T} transgenic and WT mice (late stage; N=3). Student's t test, unpaired, one-tailed. Scale bar: 25 μm. White arrow indicates one analyzed cell as an example. **c, d)** Left: quantification of nuclear bpMOK **(c)** or pBrd4 **(d)** levels (green) and DAPI staining by confocal IF of spinal cord organotypic cultures, stimulated or not with 1 μg/ml LPS overnight, from WT and SOD1^{G93A} mice (5-weeks old, N=3). Represented data

are the fold-change of nuclear bpMOK signal upon LPS stimulation normalized to the corresponding unstimulated controls. Student's t-test, unpaired, two-tailed. Right: representative images of both IF assays corresponding to each condition. Scale bar: 25 μm. **e)** Flow cytometry assessment of bpMOK expression levels in $CD11b^{+}$ cells isolated from early-onset $SOD1^{G93A}$ or WT mouse spinal cords (14-weeks old; N=9). Student's t-test, unpaired, two-tailed. **f)** Time-course body weight monitorization of $SOD1^{G93A}$ mice injected (i.p.) with C13 compound (20 μg per dose) or vehicle (N=9) starting at 11 weeks of age, thrice a week and along three weeks (grey window). All body weight values are normalized to each mouse's maximum reached weight (% of maximum). One-way ANOVA (mixed-results model) followed by Tukey post-hoc test. Data are the mean -/+ S.E.M. from 'N' independent experiments, and *P<0.05, **P<0.01 and ***P<0.001. NS: not significant.

References

1. Caballero-Hernandez, D. *et al.* The 'Omics' of Amyotrophic Lateral Sclerosis. *Trends Mol. Med.* **22**, 53–67 (2016).
2. Feldman, E. L. *et al.* Amyotrophic lateral sclerosis. *Lancet* **400**, 1363–1380 (2022).
3. Ransohoff RM. How neuroinflammation contributes to neurodegeneration. *Science* **353**, 777–783 (2016).
4. Van Harten, A. C. M., Phatnani, H. & Przedborski, S. Non-cell-autonomous pathogenic mechanisms in amyotrophic lateral sclerosis. *Trends Neurosci.* **44**, 658–668 (2021).
5. Clarke, B. E. & Patani, R. The microglial component of amyotrophic lateral sclerosis. *Brain* **143**, 3526–3539 (2020).
6. McCauley, M. E. & Baloh, R. H. Inflammation in ALS/FTD pathogenesis. *Acta Neuropathol.* **137**, 715–730 (2019).
7. Troutman, T. D., Kofman, E. & Glass, C. K. Exploiting dynamic enhancer landscapes to decode macrophage and microglia phenotypes in health and disease. *Mol. Cell* **81**, 3888–3903 (2021).
8. Yeh, H. & Ikezu, T. Transcriptional and Epigenetic Regulation of Microglia in Health and Disease. *Trends Mol. Med.* **25**, 96–111 (2019).
9. Arai, T. *et al.* TDP-43 is a component of ubiquitin-positive tau-negative inclusions in frontotemporal lobar degeneration and amyotrophic lateral sclerosis. *Biochem. Biophys. Res. Commun.* **351**, 602–611 (2006).
10. Neumann, M. *et al.* Ubiquitinated TDP-43 in Frontotemporal Lobar Degeneration and Amyotrophic Lateral Sclerosis. *Science (80-.).* **314**, 130–133 (2006).
11. Torres, P. *et al.* A motor neuron disease mouse model reveals a non-canonical profile of senescence biomarkers. *Dis. Model. Mech.* **15**, dmm049059 (2022).
12. Wood, A., Gurfinkel, Y., Polain, N., Lamont, W. & Lyn Rea, S. Molecular Mechanisms Underlying TDP-43 Pathology in Cellular and Animal Models of ALS and FTLD. *Int. J. Mol. Sci.* **22**, 4705 (2021).
13. Liao, Y.-Z., Ma, J. & Dou, J.-Z. The Role of TDP-43 in Neurodegenerative Disease. *Mol. Neurobiol.* **59**, 4223–4241 (2022).
14. Miyata, Y., Akashi, M. & Nishida, E. Molecular cloning and characterization of a novel member of the MAP kinase superfamily. *Genes to Cells* **4**, 299–309 (1999).
15. Leal-Lasarte, M. M., Franco, J. M., Labrador-Garrido, A., Pozo, D. & Roodveldt, C. Extracellular TDP-43 aggregates target MAPK/MAK/MRK overlapping kinase (MOK) and trigger caspase-3/IL-18 signaling in microglia. *FASEB J.* **31**, 2797–2816 (2017).
16. Broekhuis, J. R., Verhey, K. J. & Jansen, G. Regulation of Cilium Length and Intraflagellar Transport by the RCK-Kinases ICK and MOK in Renal Epithelial Cells. *PLoS One* **9**, e108470 (2014).
17. Aprile-Garcia, F., Tomar, P., Hummel, B., Khavaran, A. & Sawarkar, R. Nascent-protein ubiquitination is required for heat shock–induced gene downregulation in human cells. *Nat. Struct. Mol. Biol.* **26**, 137–146 (2019).

18. Garske, A. L., Peters, U., Cortesi, A. T., Perez, J. L. & Shokat, K. M. Chemical genetic strategy for targeting protein kinases based on covalent complementarity. *Proc. Natl. Acad. Sci.* **108**, 15046–15052 (2011).

19. Warde-Farley, D. *et al.* The GeneMANIA prediction server: biological network integration for gene prioritization and predicting gene function. *Nucleic Acids Res.* **38**, W214–W220 (2010).

20. Miyata, Y., Ikawa, Y., Shibuya, M. & Nishida, E. Specific Association of a Set of Molecular Chaperones Including HSP90 and Cdc37 with MOK, a Member of the Mitogen-activated Protein Kinase Superfamily. *J. Biol. Chem.* **276**, 21841–21848 (2001).

21. Liu, L., Yang, C. & Candelario-Jalil, E. Role of BET Proteins in Inflammation and CNS Diseases. *Front. Mol. Biosci.* **16**, 748449 (2021).

22. Wang, N., Wu, R., Tang, D. & Kang, R. The BET family in immunity and disease. *Signal Transduct. Target. Ther.* **6**, 23 (2021).

23. Bao, Y. *et al.* Brd4 modulates the innate immune response through Mnk2–eIF4E pathway-dependent translational control of IκBα. *Proc. Natl. Acad. Sci.* **114**, (2017).

24. Wang, H. *et al.* (+)-JQ1 attenuated LPS-induced microglial inflammation via MAPK/NFκB signaling. *Cell Biosci* **8**, 60 (2018).

25. Jung, K. H. *et al.* RNA sequencing reveals distinct mechanisms underlying BET inhibitor JQ1-mediated modulation of the LPS-induced activation of BV-2 microglial cells. *J Neuroinflamm.* **12**, 12–18 (2015).

26. Korb, E., Herre, M., Zucker-Scharff, I., Darnell, R. B. & Allis, C. D. BET protein Brd4 activates transcription in neurons and BET inhibitor Jq1 blocks memory in mice. *Nat. Neurosci.* **18**, 1464–1473 (2015).

27. Wu, S. Y., Lee, A. Y., Lai, H. T., Zhang, H. & Chiang, C. M. Phospho Switch Triggers Brd4 Chromatin Binding and Activator Recruitment for Gene-Specific Targeting. *Mol. Cell* **49**, 843–857 (2013).

28. Belkina, B. S., Nikolajczyk, G. V & Dennis, A. C. Macrophage Inflammatory Responses BET Inhibitor JQ1 Impair Mouse Inflammation: Brd2 Genetic Disruption and BET Protein Function Is Required for. *J Immunol* **190**, 3670–3678 (2013).

29. Khan, Y. M., Kirkham, P., Barnes, P. J. & Adcock, I. M. Brd4 Is Essential for IL-1b-Induced Inflammation in Human Airway Epithelial Cells. *PLoS One* **9**, e95051 (2014).

30. Malik, N. *et al.* Suppression of interferon β gene transcription by inhibitors of bromodomain and extra-terminal (BET) family members. *Biochem. J* **468**, 363–372 (2015).

31. Chen, T., Wu, D., Moskaluk, C. A. & Fu, Z. Distinct Expression Patterns of ICK/MAK/MOK Protein Kinases in the Intestine Implicate Functional Diversity. *PLoS One* **8**, e79359 (2013).

32. Wegorzewska, I., Bell, S., Cairns, N. J., Miller, T. M. & Baloh, R. H. TDP-43 mutant transgenic mice develop features of ALS and frontotemporal lobar degeneration. *Proc. Natl. Acad. Sci. U. S. A.* **106**, 18809–18814 (2009).

33. Gois, A. M., Mendonça, D. M. F., Freire, M. A. M. & Santos, J. R. In vitro and in vivo models of amyotrophic lateral sclerosis: an updated overview. *Brain Res. Bull.*

159, 32–43 (2020).

34. Deora, V. *et al.* The microglial NLRP3 inflammasome is activated by amyotrophic lateral sclerosis proteins. *Glia* **68**, 407–421 (2020).

35. Gerbino V *et al.* The Loss of TBK1 Kinase Activity in Motor Neurons or in All Cell Types Differentially Impacts ALS Disease Progression in SOD1 Mice. *Neuron* **106**, 789-805.e5 (2020).

36. Krasemann, S. *et al.* The TREM2-APOE Pathway Drives the Transcriptional Phenotype of Dysfunctional Microglia in Neurodegenerative Diseases. *Immunity* **47**, 566-581.e9 (2017).

37. Shan, X., Vocadlo, D. & Krieger, C. Mislocalization of TDP-43 in the G93A mutant SOD1 transgenic mouse model of ALS. *Neurosci. Lett.* **458**, 70–74 (2009).

38. Cai, M., Lee, K.-W., Choi, S.-M. & Yang, E. J. TDP-43 modification in the hSOD1G93A amyotrophic lateral sclerosis mouse model. *Neurol. Res.* **37**, 253–262 (2015).

39. Marino, M. *et al.* Differences in protein quality control correlate with phenotype variability in 2 mouse models of familial amyotrophic lateral sclerosis. *Neurobiol. Aging* **36**, 492–504 (2015).

40. Pasetto, L. *et al.* Targeting Extracellular Cyclophilin A Reduces Neuroinflammation and Extends Survival in a Mouse Model of Amyotrophic Lateral Sclerosis. *J. Neurosci.* **37**, 1413–1427 (2017).

41. Jeon, S.-G. *et al.* Pathological Modification of TDP-43 in Amyotrophic Lateral Sclerosis with SOD1 Mutations. *Mol. Neurobiol.* **56**, 2007–2021 (2019).

42. Rock, R. B. *et al.* Role of Microglia in Central Nervous System Infections. *Clin. Microbiol. Rev.* **17**, 942–964 (2004).

43. Barrett, J. P. *et al.* Interferon-β Plays a Detrimental Role in Experimental Traumatic Brain Injury by Enhancing Neuroinflammation That Drives Chronic Neurodegeneration. *Neurobiol. Dis.* **40**, 2357–2370 (2020).

44. Yu, C.-H. *et al.* TDP-43 Triggers Mitochondrial DNA Release via mPTP to Activate cGAS/STING in ALS. *Cell* **183**, 636-649.e18 (2020).

45. Tan, P.-H., Ji, J., Hsing, C.-H., Tan, R. & Ji, R.-R. Emerging Roles of Type-I Interferons in Neuroinflammation, Neurological Diseases, and Long-Haul COVID. *Int. J. Mol. Sci.* **23**, 14394 (2022).

46. Pong Ng, H. *et al.* CITED2 limits pathogenic inflammatory gene programs in myeloid cells. *FASEB J.* **34**, 12100–12113 (2020).

47. Liu, X. *et al.* Action by CITED2 in the Nucleus B κ Negative Feedback Regulation of NF. *J Immunol* **186**, 539–548 (2011).

48. Gun-Dong, K. *et al.* CITED2 Restrains Proinflammatory Macrophage Activation and Response. *Mol. Cell. Biol.* **38**, e00452-17 (2018).

49. Zhu, Q. *et al.* TRIM24 facilitates antiviral immunity through mediating K63-linked TRAF3 ubiquitination. *J. Exp. Med.* **217**, e20192083 (2020).

50. Lee, C.-K., Mancino, A. & Mogensen, T. H. IRF and STAT Transcription Factors - From Basic Biology to Roles in Infection, Protective Immunity, and Primary Immunodeficiencies. *Front. Immunol.* **1**, 3047 (2019).

51. Roy, E. R. *et al.* Concerted type I interferon signaling in microglia and neural cells promotes memory impairment associated with amyloid β plaques. *Immunity* **55**, 879-894.e6 (2022).

52. Xue, F., Tian, J., Yu, C., Du, H. & Guo, L. Type I interferon response-related microglial Mef2c deregulation at the onset of Alzheimer's pathology in 5×FAD mice. *Neurobiol. Dis.* **152**, 105272 (2021).

53. Rodriguez, S. *et al.* Genome-encoded cytoplasmic double-stranded RNAs, found in C9ORF72 ALS-FTD brain, propagate neuronal loss. *Sci. Transl. Med.* **13**, eaaz4699 (2021).

54. Barrett, J. P. *et al.* Traumatic Brain Injury Induces cGAS Activation and Type I Interferon Signaling in Aged Mice. *Frontiers in Immunology* vol. 12 710608 (2021).

55. Nazmi, A. *et al.* Chronic neurodegeneration induces type I interferon synthesis via STING, shaping microglial phenotype and accelerating disease progression. *Glia* **67**, 1254–1276 (2019).

56. Friedman, B. A. *et al.* Diverse Brain Myeloid Expression Profiles Reveal Distinct Microglial Activation States and Aspects of Alzheimer's Disease Not Evident in Mouse Models. *Cell Rep.* **22**, 832–847 (2018).

57. Main, B. S. *et al.* Type-1 Interferons Contribute to the Neuroinflammatory Response and Disease Progression of the MPTP Mouse Model of Parkinson's Disease. *Glia* **64**, 1590–604 (2016).

58. Wang, R., Yang, B. O. & Zhang, D. Activation of Interferon Signaling Pathways in Spinal Cord Astrocytes from an ALS Mouse Model. *Glia* **59**, 946–58 (2011).

59. Zafar, A. *et al.* BHLHE40 promotes macrophage pro-inflammatory gene expression and functions. *FASEB J* **35**, 21940 (2021).

60. Cook, M. E., Jarjour, N. N., Lin, C. C. & Edelson, B. T. Transcription Factor Bhlhe40 in Immunity and Autoimmunity. *Trends Immunol.* **41**, 1023–1036 (2020).

61. Xu, X. *et al.* Bromodomain Containing Protein 4 (BRD4) Regulates Expression of its Interacting Coactivators in the Innate Response to Respiratory Syncytial Virus expression of host defense mechanisms and remodeling genes through changes in promoter accessibility. *Front Mol. Biosci.* **8**, 728661 (2021).

62. Berson, A., Nativio, R., Berger, S. L. & Bonini, N. M. Epigenetic Regulation in Neurodegenerative Diseases. *Trends Neurosci.* **41**, 587–598 (2018).

63. Jimenez-Pacheco, A. *et al.* Epigenetic Mechanisms of Gene Regulation in Amyotrophic Lateral Sclerosis. *Adv. Exp. Med. Biol.* **978**, (2017).

64. Huang, Y. *et al.* Genetic and Environmental Effects on Gene Expression Signatures of Blood Pressure: A Transcriptome-Wide Twin Study. *Hypertension* **71**, 457–464 (2018).

65. Sopic, M. *et al.* Downregulation of mapk/mak/mrk overlapping kinase 1 in peripheral blood mononuclear cells of pediatric patients with type 1 diabetes mellitus. *J Med Biochem* **41**, 282–289 (2022).

66. García-García, R., Martín-Herrero, L., Blanca-Pariente, L., Pérez-Cabello, J. & Roodveldt, C. Immune Signaling Kinases in Amyotrophic Lateral Sclerosis (ALS) and Frontotemporal Dementia (FTD). *Int J Mol Sci.* vol. 22 13280 (2021).

67. Guo, W. *et al.* The multifaceted role of kinases in amyotrophic lateral sclerosis: genetic, pathological and therapeutic implications. *Brain* **143**, 1651–1673 (2020).

68. Herzog, V. A. *et al.* Thiol-linked alkylation of RNA to assess expression dynamics. *Nat Methods* **14**, 1198–1204 (2017).

69. Neumann, T. *et al.* Quantification of experimentally induced nucleotide conversions in high-throughput sequencing datasets. *BMC Bioinforma.* **20**, 258 (2019).

70. Araldi, E. *et al.* Lanosterol Modulates TLR4-Mediated Innate Immune Responses in Macrophages. *Cell Rep.* **19**, 2743–2755 (2017).

71. Enesa, K. *et al.* Pellino1 Is Required for Interferon Production by Viral Double-stranded RNA. *J. Biol. Chem.* **287**, 34825–34835 (2012).

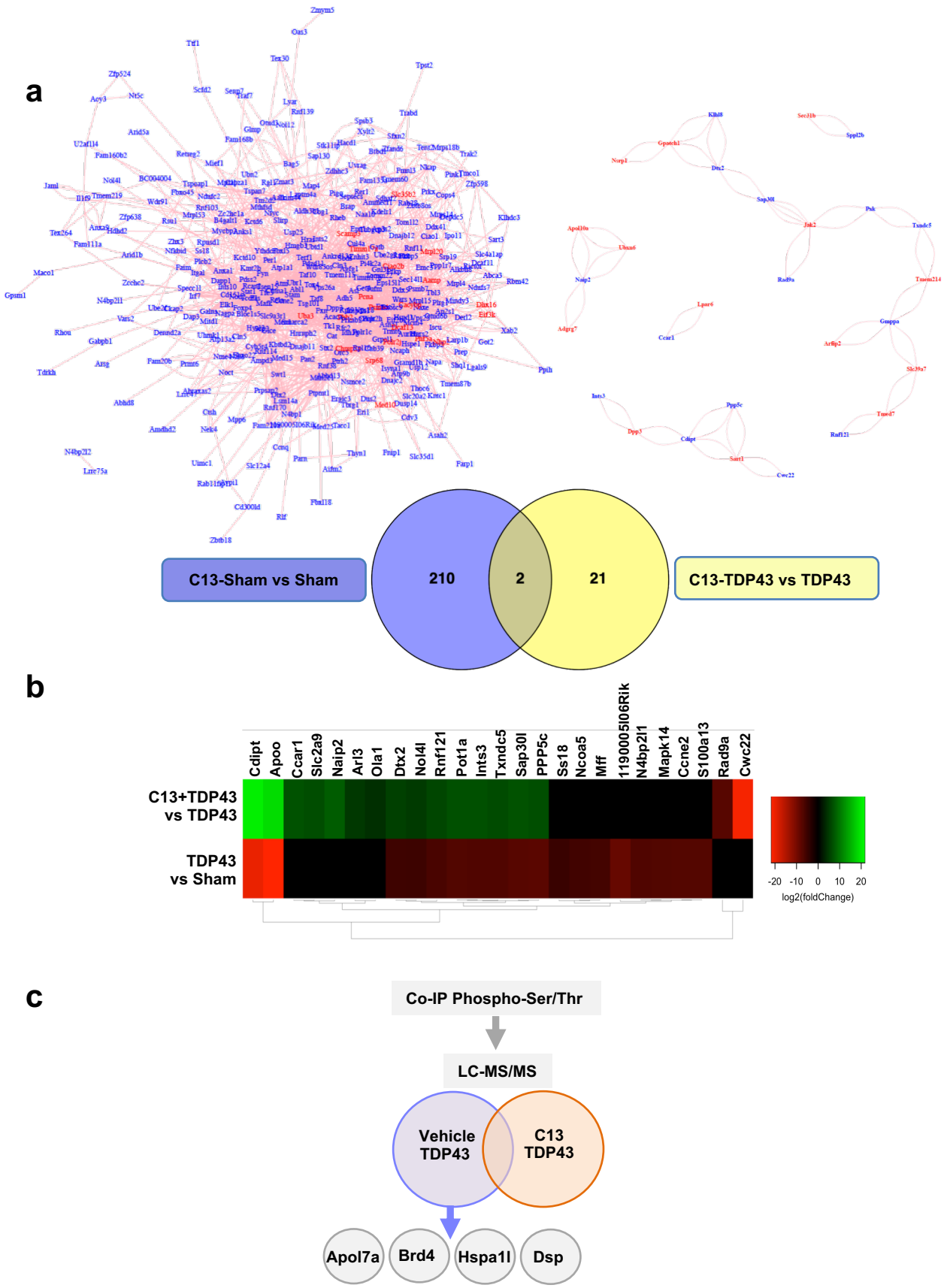
a
C13-Sham vs Sham
210
2
21
C13-TDP43 vs TDP43
b
Cdipt
Apoo
Ccar1
Slc2a9
Naip2
Arl3
Ola1
Dtx2
Nol4l
Rnf121
Pot1a
Ints3
Txndc5
Sap30l
PPP5c
Ss18
Ncoa5
Mff
1190005I06Rik
N4bp2l1
Mapk14
Ccne2
S100a13
Rad9a
Cwc22
C13+TDP43 vs TDP43
TDP43 vs Sham
-20 -10 0 10 20
log2(foldChange)
c
Co-IP Phospho-Ser/Thr
LC-MS/MS
Vehicle TDP43
C13 TDP43
Apol7a
Brd4
Hspa1l
Dsp

Figure 1

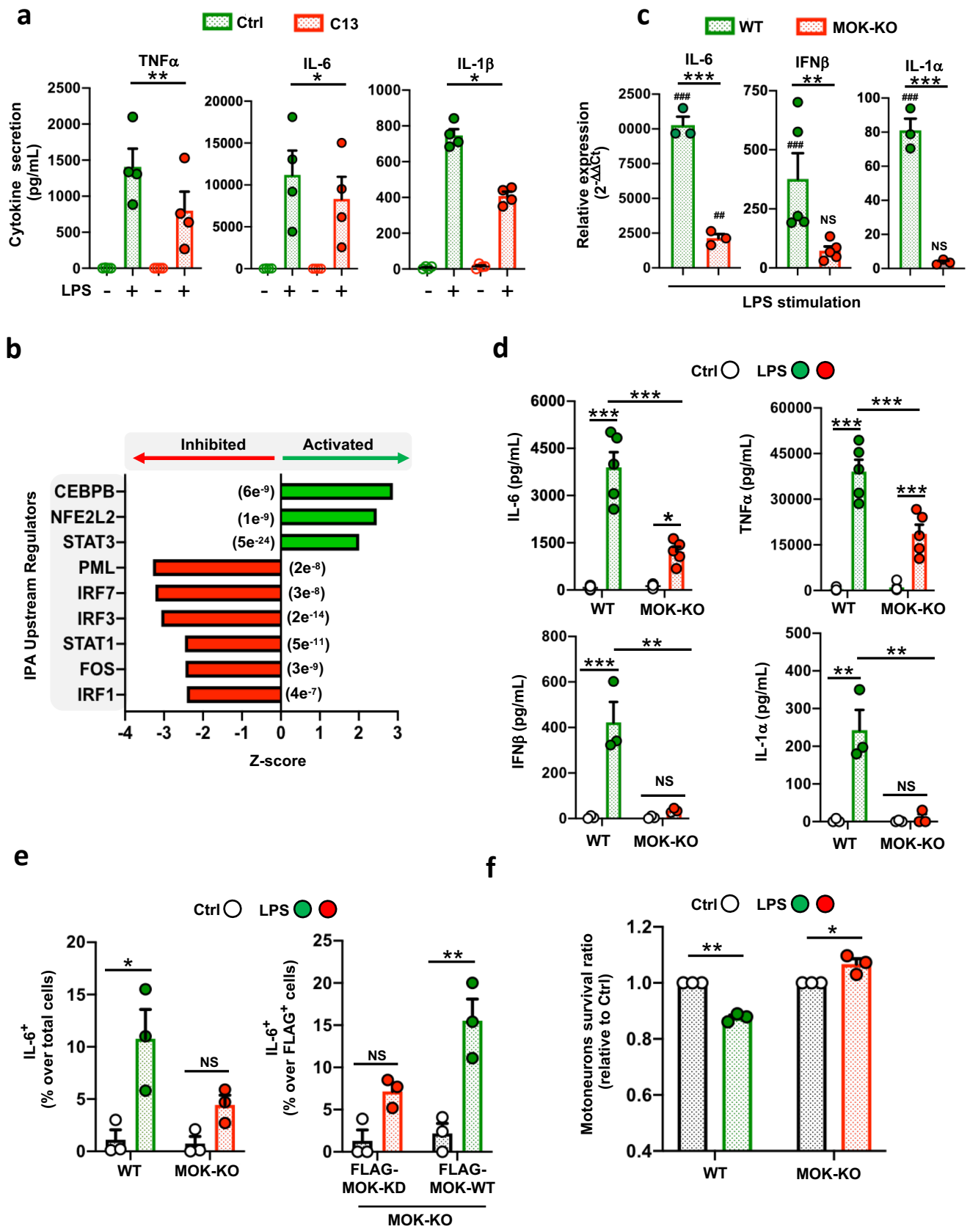
a
Ctrl
C13
TNFα
IL-6
IL-1β
Cytokine secretion (pg/mL)
LPS
c
WT
MOK-KO
IL-6
IFNβ
IL-1α
Relative expression ($2^{-\Delta\Delta Ct}$)
LPS stimulation
b
Inhibited
Activated
IPA Upstream Regulators
CEBPB
NFE2L2
STAT3
PML
IRF7
IRF3
STAT1
FOS
IRF1
Z-score
d
Ctrl
LPS
IL-6 (pg/mL)
TNFα (pg/mL)
IFNβ (pg/mL)
IL-1α (pg/mL)
WT
MOK-KO
e
IL-6+ (% over total cells)
IL-6+ (% over FLAG+ cells)
FLAG-MOK-KD
FLAG-MOK-WT
MOK-KO
f
Motoneurons survival ratio (relative to Ctrl)

Figure 2

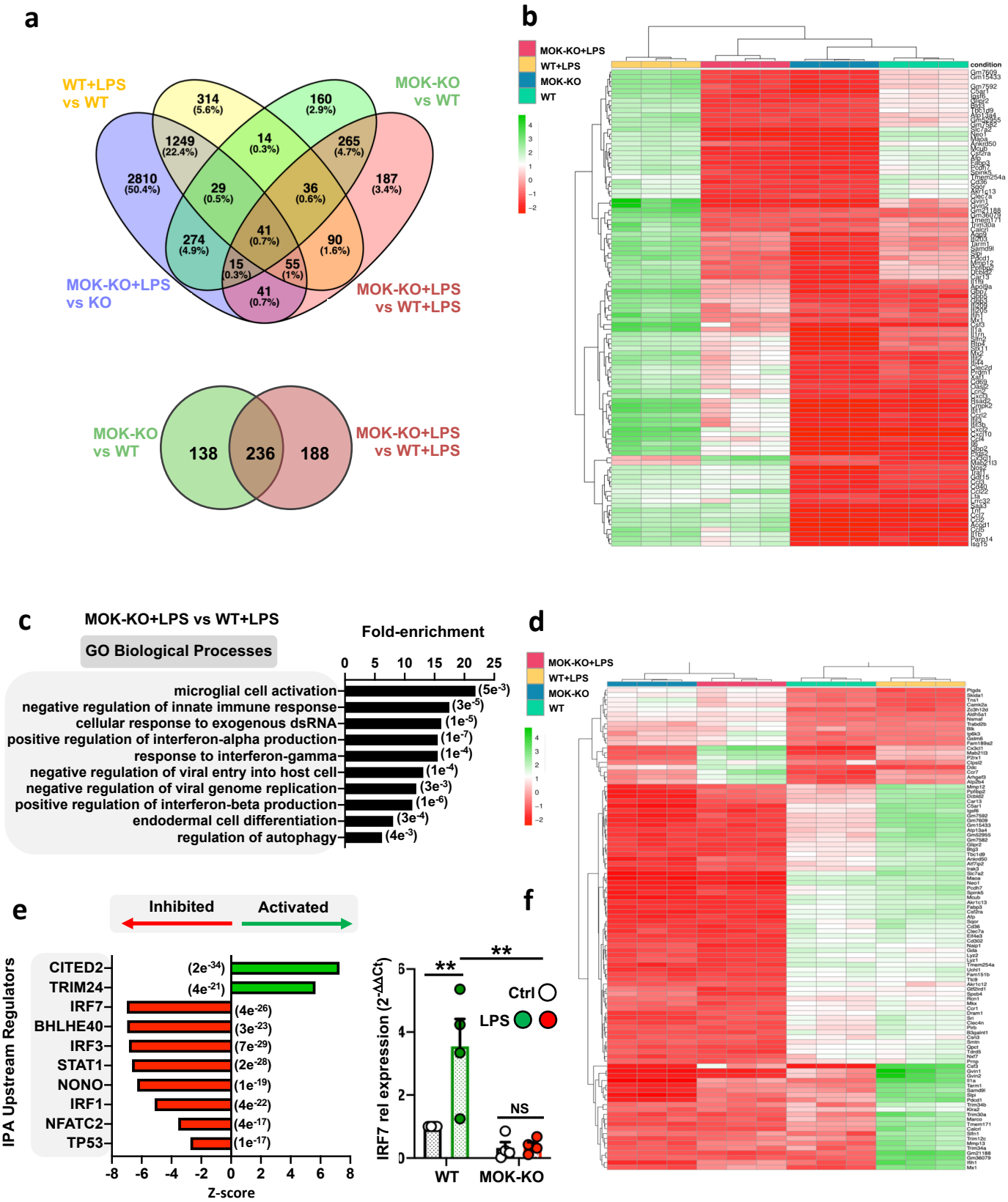
a
WT+LPS vs WT
MOK-KO vs WT
MOK-KO+LPS vs KO
MOK-KO+LPS vs WT+LPS
314 (5.6%)
160 (2.9%)
1249 (22.4%)
14 (0.3%)
265 (4.7%)
2810 (50.4%)
29 (0.5%)
36 (0.6%)
187 (3.4%)
41 (0.7%)
274 (4.9%)
90 (1.6%)
15 (0.3%)
55 (1%)
41 (0.7%)
MOK-KO vs WT
138
236
188
MOK-KO+LPS vs WT+LPS
b
MOK-KO+LPS
WT+LPS
MOK-KO
WT
condition
c
MOK-KO+LPS vs WT+LPS
GO Biological Processes
Fold-enrichment
0 5 10 15 20 25
microglial cell activation (5e-3)
negative regulation of innate immune response (3e-5)
cellular response to exogenous dsRNA (1e-5)
positive regulation of interferon-alpha production (1e-7)
response to interferon-gamma (1e-4)
negative regulation of viral entry into host cell (1e-4)
negative regulation of viral genome replication (3e-3)
positive regulation of interferon-beta production (1e-6)
endodermal cell differentiation (3e-4)
regulation of autophagy (4e-3)
d
MOK-KO+LPS
WT+LPS
MOK-KO
WT
e
Inhibited
Activated
IPA Upstream Regulators
CITED2 (2e-34)
TRIM24 (4e-21)
IRF7 (4e-26)
BHLHE40 (3e-23)
IRF3 (7e-29)
STAT1 (2e-28)
NONO (1e-19)
IRF1 (4e-22)
NFATC2 (4e-17)
TP53 (1e-17)
-8 -6 -4 -2 0 2 4 6 8
Z-score
f
IRF7 rel expression (2-ΔΔCt)
0 2 4 6
**
**
NS
Ctrl
LPS
WT
MOK-KO

Figure 3

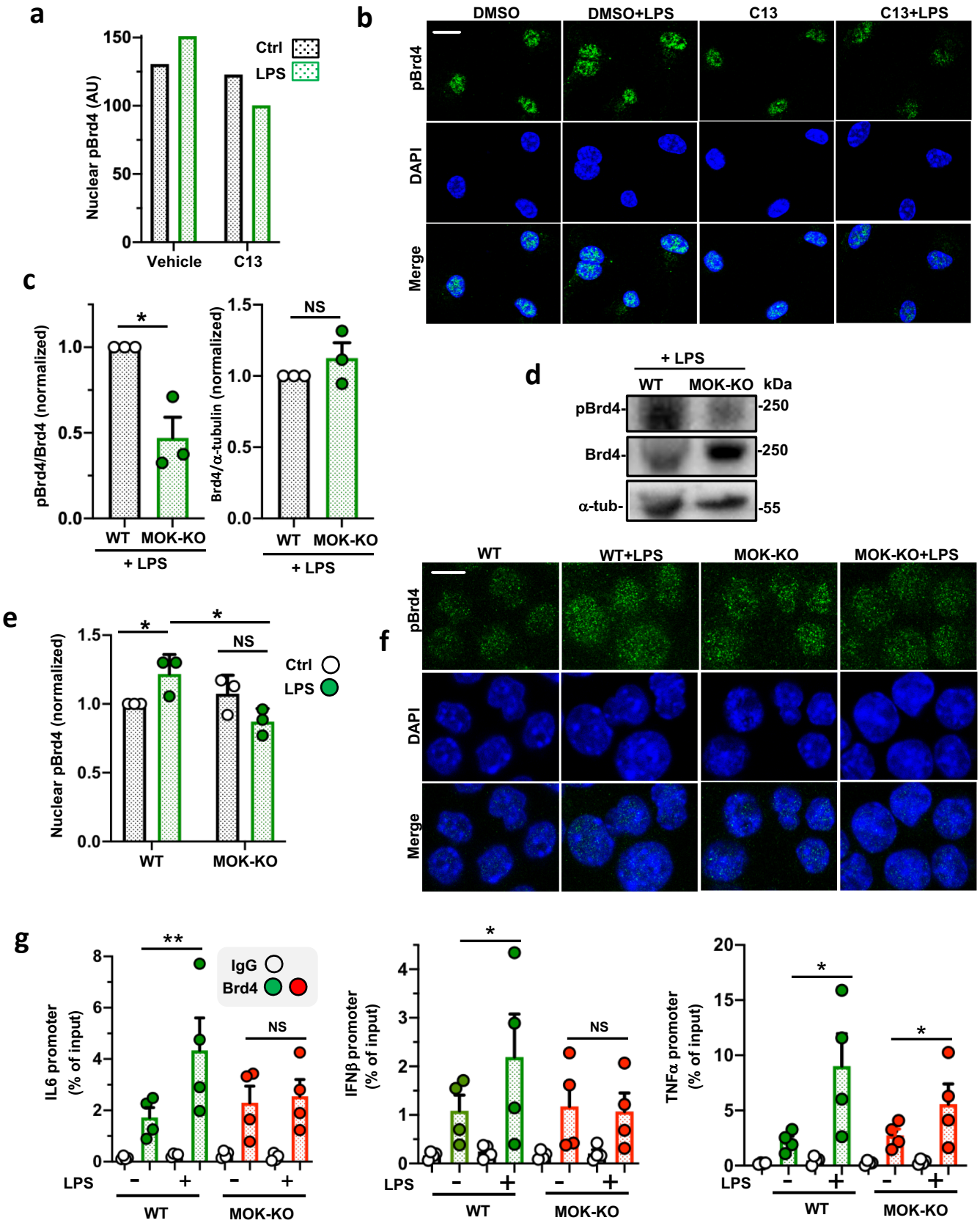
a
Nuclear pBrd4 (AU)
150
100
50
0
Ctrl
LPS
Vehicle
C13
b
DMSO
DMSO+LPS
C13
C13+LPS
pBrd4
DAPI
Merge
c
pBrd4/Brd4 (normalized)
1.0
0.5
0.0
*
WT
MOK-KO
+ LPS
Brd4/α-tubulin (normalized)
1.5
1.0
0.5
0.0
NS
WT
MOK-KO
+ LPS
d
+ LPS
WT
MOK-KO
kDa
pBrd4-
-250
Brd4-
-250
α-tub-
-55
e
Nuclear pBrd4 (normalized)
1.5
1.0
0.5
0.0
*
*
NS
Ctrl
LPS
WT
MOK-KO
f
WT
WT+LPS
MOK-KO
MOK-KO+LPS
pBrd4
DAPI
Merge
g
IL6 promoter (% of input)
8
6
4
2
0
**
NS
IgG
Brd4
LPS
-
+
-
+
WT
MOK-KO
IFNβ promoter (% of input)
4
3
2
1
0
*
NS
LPS
-
+
-
+
WT
MOK-KO
TNFα promoter (% of input)
20
15
10
5
0
*
*
LPS
-
+
-
+
WT
MOK-KO

Figure 4

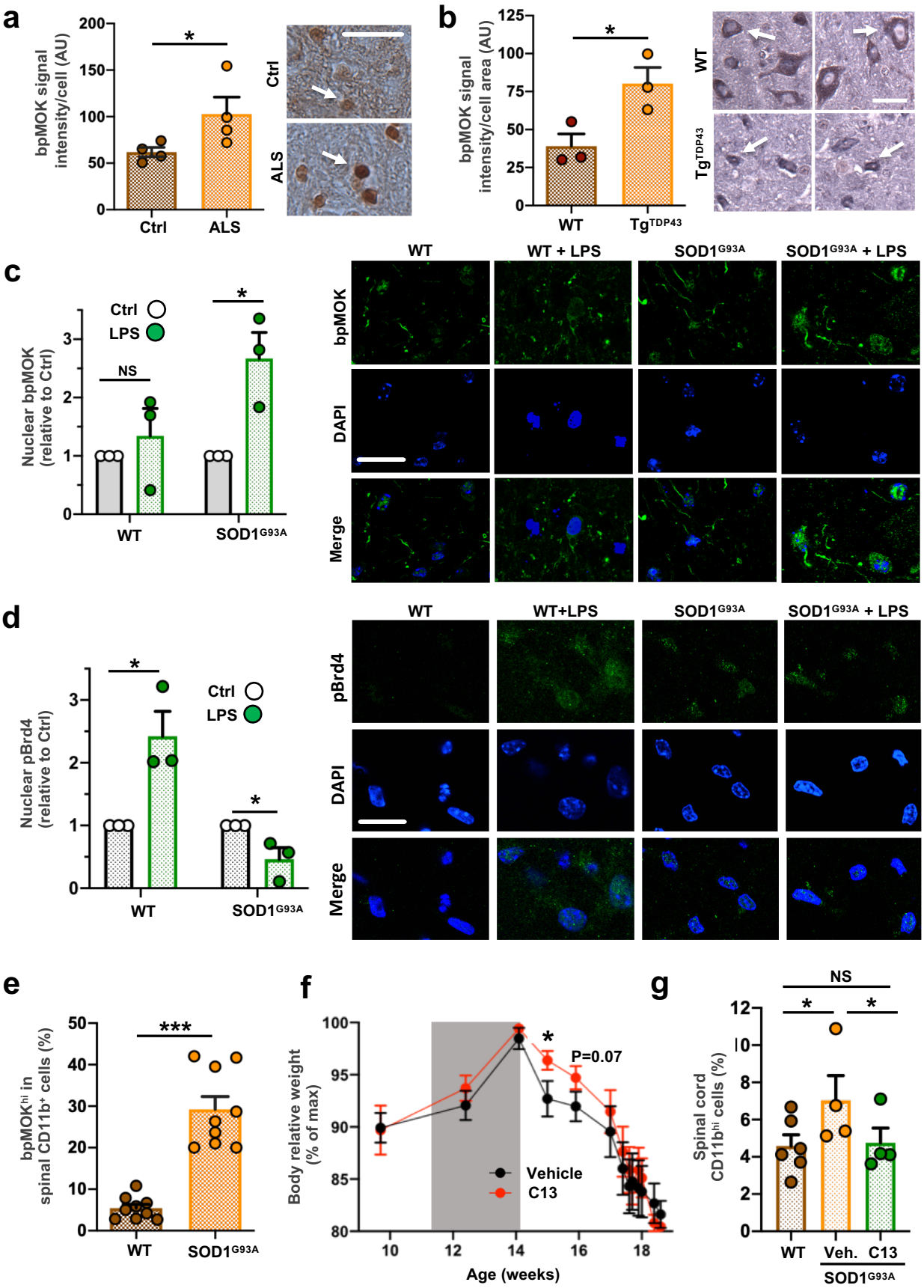
a
bpMOK signal intensity/cell (AU)
200
150
100
50
0
*
Ctrl
ALS
Ctrl
ALS
b
bpMOK signal intensity/cell area (AU)
125
100
75
50
25
0
*
WT
TgTDP43
WT
TgTDP43
c
Nuclear bpMOK (relative to Ctrl)
Ctrl
LPS
NS
*
WT
SOD1G93A
WT
WT + LPS
SOD1G93A
SOD1G93A + LPS
bpMOK
DAPI
Merge
d
Nuclear pBrd4 (relative to Ctrl)
Ctrl
LPS
*
*
WT
SOD1G93A
WT
WT+LPS
SOD1G93A
SOD1G93A + LPS
pBrd4
DAPI
Merge
e
bpMOKhi in spinal CD11b+ cells (%)
***
WT
SOD1G93A
f
Body relative weight (% of max)
*
P=0.07
Vehicle
C13
Age (weeks)
g
Spinal cord CD11bhi cells (%)
NS
*
*
WT
Veh.
C13
SOD1G93A

Figure 5